

1 **Gas seepage and pockmark formation from subsurface**
2 **reservoirs: Insights from table-top experiments**

3 **I. Vaknin¹, E. Aharonov^{1*}, R. Holtzman^{2*}, O. Katz³**

4 ¹Institute of Earth Sciences, The Hebrew University of Jerusalem, Jerusalem, Israel

5 ²Centre for Fluid and Complex Systems, Coventry University, Coventry, United Kingdom

6 ³Geological Survey of Israel, Jerusalem, Israel

7 **Key Points:**

- 8 • Sandbox experiments link pockmark morphology (irregular vs conical) to gas-seepage-
9 induced deformation of the host (seal) layer
- 10 • Experiments and theory show seal thickness and consolidation control deformation
11 mechanism: doming, brittle (faults), or plastic (bubbles)
- 12 • Theoretical calculations predict that under field conditions, the preferred mech-
13 anism for gas escape will be bubbles rising in faults.

Corresponding author: Einat Aharonov, Ran Holtzman, einatah@mail.huji.ac.il,
ran.holtzman@coventry.ac.uk

Abstract

Pockmarks are morphological depressions commonly observed in ocean and lake floors. Pockmarks form by fluid (typically gas) seepage through a sealing sedimentary layer, deforming and breaching the layer. The seepage-induced sediment deformation mechanisms, and their links to the resulting pockmarks morphology, are not well understood. To bridge this gap, we conduct laboratory experiments in which gas seeps through a granular (sand) reservoir, overlaid by a (clay) seal, both submerged under water. We find that gas rises through the reservoir and accumulates at the seal base. Once sufficient gas overpressure is achieved, gas deforms the seal, and finally escapes via either: (i) doming of the seal followed by dome breaching via fracturing; (ii) brittle faulting, delineating a plug. The gas lifts the plug and seeps through the bounding faults; or (iii) plastic deformation by bubbles ascending through the seal. The preferred mechanism is found to depend on the seal thickness and stiffness: in stiff seals, a transition from doming and fracturing to brittle faulting occurs as the thickness increases, whereas bubbles rise is preferred in the most compliant, thickest seals. Seepage can also occur by mixed modes, such as bubbles rising in faults. Repeated seepage events suspend the sediment at the surface and create pockmarks. We present a quantitative analysis that explains the tendency for the various modes of deformation observed experimentally. Finally, we connect simple theoretical arguments with field observations, highlighting similarities and differences that bound the applicability of laboratory experiments to natural pockmarks.

Plain Language Summary

Pockmarks are pit-like depressions common in ocean and lake floors, formed by gas seepage through underlying sediments. Despite relevance to both fossil fuel exploration and global warming, the mechanisms by which pockmarks evolve remain elusive. We conduct simple laboratory experiments in which we inject air into a layer of glass beads ("reservoir") overlain by a layer of clay ("seal"), all submerged underwater in a transparent box. We find that gas rises through the sand and accumulates at the base of the clay. Then, gas pressure rises until it suffices to deform the clay and escape, forming a pockmark. This occurs by one of three mechanisms, depending on clay thickness and stiffness: (i) heaving of a dome which then fractures in thin clay layers; (ii) faulting in thick, stiff clays; and (iii) bubbles ascend in thick, soft clays. Pipe-like focused gas conduits connecting the clay bottom to the pockmark are created by the rise of a "trains" of bubbles that weaken their path. These pathways can also initiate in faults. Repeated seepage events push the clay particles, suspending them in water to create a pockmark. Our findings agree with field observations, improving our understanding of natural pockmark formation.

1 Introduction

Gas seepage from oceanic and lacustrine sediments is globally prevalent, forming geological structures such as pockmarks, vents, and mud volcanoes along the continental margins at many locations (Dupré et al., 2010; Schattner et al., 2012; Skarke et al., 2014; King & MacLean, 1970; Pilcher & Argent, 2007; Sultan et al., 2010; Q. Sun et al., 2012; Hovland et al., 2005; Riedel et al., 2020; de Mahiques et al., 2017; Krämer et al., 2017). Oceanic gas seeps introduce large quantities of methane into the water body, up to ~ 65 Tg/yr from continental shelves alone (Skarke et al., 2014; Hovland et al., 1993). Methane venting affects ocean acidification, de-oxygenation, and thus the global climate (Archer et al., 2009; McGinnis et al., 2006; Hornbach et al., 2004; Svensen et al., 2004). In particular, methane, a highly potent greenhouse gas, has a crucial role in the global carbon cycle and has been proposed as the cause of past episodes of climate change (e.g. Dickens, n.d.; Archer et al., 2009; Westbrook et al., 2009). Many seeps originate from oil and gas reservoirs as well as methane hydrate deposits, and thus can serve to indicate their location (Abrams, 2005). These make the study of gas seeps “one of the most important fields in marine geology” (Berndt, 2005).

Gas seepage from the seafloor occurs via two main mechanisms: (i) diffuse capillary invasion through the sediment pores (especially in coarse-grained sediments); or (ii) focused preferential flow paths, along pre-existing faults and cracks or “pipes” opened by deformation induced by the fluids themselves as they migrate (Jain & Juanes, 2009; Fauria & Rempel, 2011; Holtzman et al., 2012; Z. Sun & Santamarina, 2019). The latter typically release large amounts of gas in an episodic and/or cyclic manner (Hovland et al., 2002, 2010), and are associated with pockmarks as well as vents and mud volcanoes. Pockmarks (PMs) are of particular importance due to their abundance as well as their role as markers for gas-induced sediment deformation and breaching which leads to seepage (King & MacLean, 1970; Schattner et al., 2016). Despite the importance of PMs as the surficial manifestation of the gas seepage, the mechanisms and the consequent spatiotemporal signature of the seeps remain elusive (Hovland et al., 2010). Here, we use laboratory experiments and theoretical analysis to expose the links between gas-induced sediment deformation, seepage, pockmark formation and their spatiotemporal evolution.

1.1 Field observations of pockmarks and gas pipes

Pockmarks are depressions within the surface of oceanic and lacustrine sediments, where their formation mechanism is believed to be tightly linked to the fluid seepage mechanism feeding them (King & MacLean, 1970; Schattner et al., 2016). PM diameters can range between meters and hundreds of meters. They are widespread in continental shelves (Schattner et al., 2012; Schattner et al., 2016), slopes (Bøe et al., 1998; Gay et al., 2006; Pilcher & Argent, 2007), the deep abyss (Camerlenghi et al., 1995; A. G. Judd, 2003), deep-sea fans (Bayon et al., 2009; Loncke & Mascle, 2004), lakes, bays, estuaries (García-Gil, 2003) and fjords (Hovland et al., 2002; Forwick et al., 2009). Within seismic cross-sections, PMs are often associated with feeding pipes of incoherent signature, which suggest gas presence or liquefied or disturbed sediments (e.g. Cartwright & Santamarina, 2015).

Field observations suggest that the morphology, spatial distribution, and temporal characteristics of PMs are controlled by the geological context in which they are formed (Pilcher & Argent, 2007). Their presence and morphology are tightly linked to the fluid escape mechanisms that feed them (Cartwright et al., 2007). Pockmarks can be generally categorized according to their morphology into two types (Fig. 1): (i) conical depressions termed “Type-1”; and (ii) shallower, more irregular and distorted “Type-2” pockmarks (Riboulot et al., 2016). In Type-1, the sediment in the center of the structure is completely removed or in suspension, while the pockmark walls retain an angle of repose; this suggests that the sediment underwent a more granular or plastic defor-

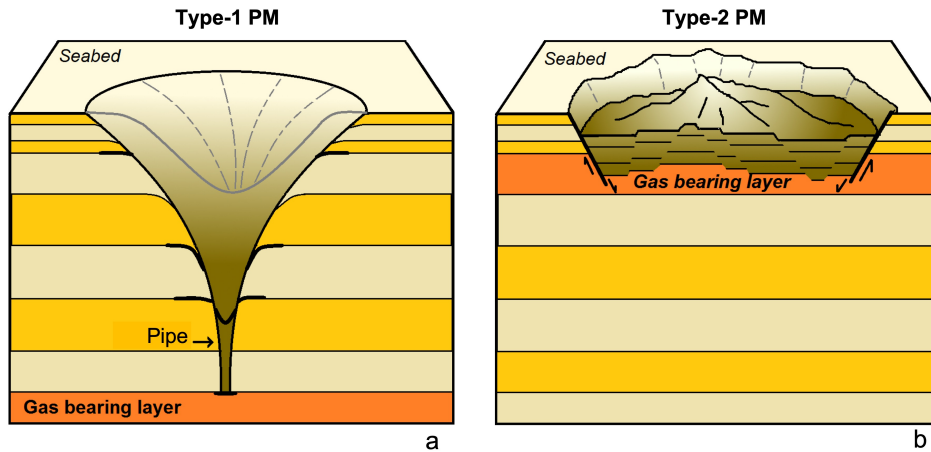


Figure 1: Geometrical characteristics of the two types of pockmarks: (a) Type-1 pockmarks are circular depression, associated with a gas pipe; (b) Type-2 pockmarks are irregular and distorted depressions.

101 mation (Cathles et al., 2010). In contrast, in Type-2 pockmarks both the original strata
 102 and the disrupting faults are easily recognized, suggesting a more solid-like or brittle de-
 103 formation. The significant difference in the structure of the two types suggests a differ-
 104 ent formation mechanism, such as the origin of the emitted gas: Type-1 usually origi-
 105 nates from deeper oil and gas reservoirs (Cathles et al., 2010), whereas Type-2 has been
 106 associated with near-surface gas hydrate layers (Riboulot et al., 2016). Although Type-
 107 2 pockmarks are found in many sites (Dillon et al., 1998; Sultan et al., 2010; Macelloni
 108 et al., 2012; Simonetti et al., 2013; Riboulot et al., 2016) they are far less common than
 109 Type-1.

110 1.2 Potential formation mechanisms of pipes and pockmarks

111 Several mechanisms have been proposed for the formation of fluid escape features
 112 and their associated pockmark structures (Cartwright & Santamarina, 2015):

113 (i) **Hydraulic fracturing**: this mechanism assumes fluid overpressure within or
 114 under a brittle sediment layer. If the fluid pressure rises, it may fracture the overlying
 115 seal, propagating a network of hydraulic fractures toward the surface. The accumulated
 116 and connected fractures form a breccia pipe. Growth in this case is suggested to culmi-
 117 nate in explosive venting, leaving a dent at the surface (Moss & Cartwright, 2010; Plaza-
 118 Faverola et al., 2010, 2011; Løseth et al., 2011; Davies et al., 2012). We note that this
 119 mechanism is not supported by laboratory experiments.

120 (ii) **Capillary barriers forming a flat piston**: in this mechanism, proposed by
 121 Cathles et al. (2010), gas rises in a water-saturated reservoir and accumulates at its top,
 122 capped by an overlying low permeability seal. Since the seal is water-saturated and has
 123 a much smaller grain size than the underlying reservoir, the gas-water interface at the
 124 base of the seal forms a “capillary barrier” (Morel-Seytoux, 1993) which resists both the
 125 ascent of gas and the descent of water. As gas pressure rises it will plastically deform
 126 the seal, forming an upward-propagating capillary barrier that acts as a flat-roofed gas
 127 “piston”. The invasion and upward propagation of the piston requires liquefaction of the
 128 sediment in front of it (Varas et al., 2011; Ramos et al., 2015). Cathles et al. (2010) es-
 129 timated that once the piston ascends halfway to the surface its ascent accelerates, and
 130 once the piston gets close to the seafloor a PM of width similar to the piston forms rapidly.

131 Although in our experiments (below) we do observe the formation of pistons at the reservoir-
 132 seal interface, they do not propagate towards the surface, as predicted by Cathles et al.
 133 (2010). (Nor are we aware of any previous experiments in which a piston ascends.)

134 **(iii) Erosive fluidization:** sediment fluidization occurs when pressure gradients
 135 exerted by pore fluids on sediment grains (“seepage forces”) exceed the lithostatic stress
 136 that holds the grains in place. Seepage induced fluidization has been suggested to form
 137 PMs and mud volcanoes (Brown, 1990; Nermoen et al., 2010). Within this mechanism,
 138 one can include also the “pore-fluid escape” mechanism that occurs during compaction-
 139 induced dewatering (Harrington, 1985; Böttner et al., 2019). Cone-shaped structures,
 140 which widen towards the surface, such as the Type-1 PMs and the associated feeding pipe
 141 in Fig. 1A, are often observed in the field (Riboulot et al., 2016). Similar cone-shaped
 142 structures have been shown experimentally to form under a high upwards fluid flux through
 143 submerged grain layers (Varas et al., 2009, 2011; Ramos et al., 2015). Such seepage-driven
 144 pipe formation may explain why pipes have a minimum distance between them, set by
 145 a lateral drainage distance from the overpressurized gas zone (Moss & Cartwright, 2010).
 146 If near-surface sediment is fluidized, grains may be ejected to the water column and de-
 147 posited on the PM crater shoulders (Varas et al., 2009). Such sediment ejection in nat-
 148 ural PMs is indicated by sonar data from the North Sea indicating massive plumes of
 149 suspended sediments above pockmarks (A. Judd & Hovland, 2009). Despite the support-
 150 ing morphological field evidence, this mechanism remains controversial as it was argued
 151 that the initiation of seepage-induced fluidization requires high fluid seepage velocity (i.e.
 152 a jet) that cannot be initiated in layered sediments (Cartwright & Santamarina, 2015).

153 **(iv) Decompaction:** Two-phase systems consisting of grains and a liquid (with
 154 no gas) have shown the spontaneous formation of high permeability fluid escape pipes,
 155 forming by decompaction of the grains at the tip of upwelling bubbles (“solitons”) com-
 156 prising buoyant fluids (Räss et al., 2018). When rising pipes reach the surface they form
 157 pockmarks. This process requires non-linear rheology of the sediments and has not yet
 158 been observed experimentally.

159 **(v) Flow along existing fractures:** gas utilizes existing high permeability faults
 160 and fractures to escape from depth (Hustoft et al., 2007; Berndt et al., 2003; Lawal et
 161 al., 2023). This process, comprising gas ascent in “pockets”, followed by the collapse of
 162 fluid-filled cavities or conduits, (also evident in some of our experiments described be-
 163 low), was used to explain observed microseismic events below the Marmara sea (Tary
 164 et al., 2012).

165 **(vi) Gas hydrate dissociation and volume loss:** This mechanism considers
 166 a large body of gas hydrates that accumulates under, and initially inflates (forming a dome),
 167 an overlying layer of low permeability sediments. If the hydrates dissociate due to changes
 168 in temperature or pressure, the region may collapse, creating an irregular crater (Riboulot
 169 et al., 2016). This is hypothesized as the mechanism forming Type-2 PMs and based on
 170 seismic data of pockmarks from the Niger Delta where gas hydrates are abundant. We
 171 point out that free gas, even with no gas hydrate source, can also form a dome in soft
 172 sediments simply by buoyancy, as observed in offshore New Zealand (Koch et al., 2015),
 173 such that the consequent emergence of gas seeps and dome failure can produce Type-
 174 2 PMs, as will be shown in the experimental results below.

175 1.3 Nature of seepage through natural pockmarks

176 Continuous measurements of pockmark activity in the field are rare, thus the mode
 177 of activity of most PMs is uncertain. Observations suggest both continuous seepage (Hovland
 178 & Sommerville, 1985; A. Judd & Hovland, 2009) and episodic activity (Field & Jennings,
 179 1987; Hasiotis et al., 1996; Soter, 1999; Franchi et al., 2017; Goff, 2019; Jedari-Eyvazi
 180 et al., 2023) exist at different PM locations. Linke et al. (1999) measured many orders
 181 of magnitude variability in seepage rates at the Cascadia accretionary complex. Hovland

182 et al. (2002) suggest that most PMs exhibit dormancy as a quiescent period between ac-
 183 tivities. The source of this gas flux variability is uncertain.

184 **1.4 Experimental and numerical simulations of pockmarks and pipes**

185 Experiments can aid in determining which of the above multiple proposed mech-
 186 anisms control the sediment breaching and associated seepage and PM formation, and
 187 under which conditions each mechanism dominates. In addition, experiments can im-
 188 prove understanding of the temporal and spatial evolution of PMs. Previous experimen-
 189 tal studies of gas-related sediment breaching and PM formation mainly used a homo-
 190 geneous granular medium (i.e. a single water-saturated granular layer), injecting gas at
 191 its bottom (Varas et al., 2009, 2011; Nermoen et al., 2010; Fauria & Rempel, 2011; Ramos
 192 et al., 2015; Poryles et al., 2016). For such settings, Varas et al. (2009) showed that if
 193 the injection rate is low enough, gas bubbles can ascend through the granular layer in-
 194 termittently (one at a time). The zone through which the bubbles pass is fluidized, cre-
 195 ating a cone-shaped fluidized pipe, where the wide part of the cone defines the crater near
 196 the surface (i.e., a Type 1 PM). The transition from capillary gas seepage (at high ef-
 197 fective stress) to fracture and Type-1 PM formation (at low effective stress) has been re-
 198 produced in laboratory experiments by injecting gas into submersed unconsolidated coarse-
 199 grained sediments, and tuning the level of overpressure (and by this the level of effec-
 200 tive stress) (Fauria & Rempel, 2011). Investigating further the influence of effective stress
 201 on deformation mode, considering the general process of gas seepage from sediments (not
 202 specifically PM formation), Z. Sun and Santamarina (2019) found that gas ascends in
 203 bubbles when the imposed confining stress is low, while it produces gas-transmitting frac-
 204 tures at higher confinement.

205 Fewer studies considered layering with a low permeability barrier. Mazzini et al.
 206 (2008) injected gas at the bottom of a 2D cell filled with porous granular media over-
 207 laid by a thin layer of clay. Gas accumulated beneath the clay until a critical overpres-
 208 sure was reached, leading to (i) doming at the interface between the two layers and (ii)
 209 lateral migration of the gas along the interface. Further gas injection led to dome frac-
 210 turing and gas escape. Barry et al. (2012) considered similar layered settings, showing
 211 that thin-plate elasticity theory can predict the flexure and doming of the sediment layer
 212 vs. the applied gas pressure. Specifically, the authors link gas overpressure to dome ge-
 213 ometry and material intrinsic mechanical properties (Eq. 1 in Ugural (1999).) Barry
 214 et al. (2012) found that a small deflection can already cause sediment fracture in nat-
 215 ural domes, which may indicate why pockmarks readily form in fine-grained sediments.
 216 It was hypothesized that doming represents an early phase of pockmark formation (A. Judd
 217 & Hovland, 2009).

218 **1.5 This study: Open questions and our approach**

219 The above-noted studies advance the understanding of coupled gas-seepage and sed-
 220 iment deformation, and consequent PM formation. Yet, to date, there is no experimen-
 221 tal exploration of the PM formation process as a whole, from its initiation, e.g. forma-
 222 tion of gas conduits from the reservoir, to gas-induced sediment breaching, PM forma-
 223 tion, and gas seepage. In particular, we identify the following open questions: What are
 224 the mechanical conditions for PM formation? How does PM morphology evolve with time?
 225 Is seepage through the PM episodic or continuous? How do PMs tap gas from deeply
 226 buried reservoirs? How are different PM morphologies created? What determines the
 227 size of a PM? What is the geometrical and mechanical connection between a PM and
 228 its feeding pipes?

229 In this paper, we present a simple experimental setup, that allows us to examine
 230 the deformation mechanisms and PM evolution under various settings. Our experimen-
 231 tal data, which are in good agreement with theory, explain the formation process of pref-

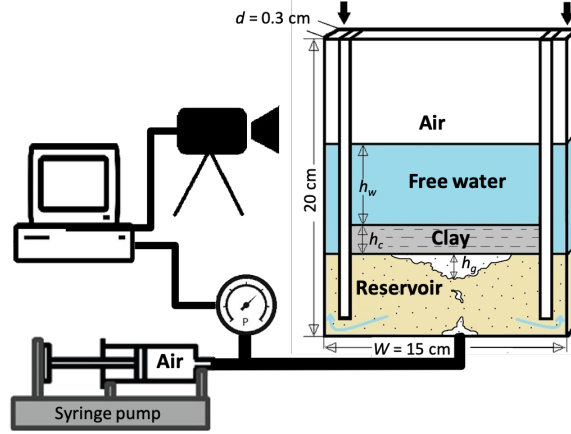


Figure 2: Schematics of the experimental setting: A quasi two-dimensional (2D) cell (thickness $d = 0.3$ cm) made of a Plexiglas transparent box, containing a thin layer of low-permeability granular media (clay) overlaying a more permeable reservoir layer (glass beads), both saturated with water. Gas (here, air) is injected using a syringe pump (where gas pressure is recorded) from a point through the lower face of the cell. Time-lapse images track the sediment deformation. Partitions at sides are used to allow free water drainage (wide arrows), ensuring that overpressure is due to the gas only (avoiding hydrofracturing). We use 2 experimental cell widths, W , 15 and 50 cm.

232 entential seepage pathways and the episodic, multi-stage, nature of PM generation, and
 233 shed light on how different sediment breaching mechanisms result in different types of
 234 PMs. Finally, we compare our results to field observations of pockmarks, presenting a
 235 simple theoretical analysis that exposes differences and similarities between laboratory
 236 and field settings and helps evaluate the applicability of laboratory experiments to nat-
 237 ural pockmarks.

238 2 Experimental setup: Table-top pockmarks

239 We model submarine gas seepage using a rectangular, quasi-2D transparent Plex-
 240 iglas cell (15 x 20 x 0.3 cm), filled with two water-saturated granular layers of signifi-
 241 cantly different grain size and hence permeability, acting as a reservoir overlaid by a seal
 242 (Fig. 2). All layers are submerged in water. Air is injected through a point at the center
 243 beneath the bottom layer by a syringe pump. Images of the injected gas-induced sedi-
 244 ment deformation during the experiments are captured using a high-resolution monochrome
 245 camera at 10 Hz. The injected air pressure was measured and recorded at 1 Hz at the
 246 syringe end. Experiments ran until a stable pockmark was achieved. A clear PM struc-
 247 ture was usually formed within 30-60 minutes, however run-time in most of the exper-
 248 iments did not exceed 75 minutes, a technical limitation set by the storage capacity. To
 249 test the scalability of the experiments, namely the dependence of our results on the sys-
 250 tem size, a few experiments were repeated with a larger cell (52 x 26 x 0.3 cm), record-
 251 ing images at 5 Hz.

252 The bottom (“reservoir”) layer consists of tightly packed glass beads (RETSCH;
 253 diameter range 0.75-1 mm). To ensure a uniform and repeatable packing, after pouring
 254 the beads, as they start submerging, the cell was shaken vertically by hand until the beads
 255 locked and the matrix solidified. The overlaying (“seal”) layer consists of natural kaoli-
 256 nite clay (Sigma-Aldrich) poured into the cell in suspension (fluidized in water), left to
 257 settle for either 3 or 6 weeks, to test the effect of the degree of consolidation and seal rigid-

Table 1: Summary of experimental conditions and results.

Test # ^a	Clay (cm)	Sand (cm)	Water (cm)	Settle time, t_s (weeks)	Failure mode ^b	Pockmark type	Run time (min.)
4A	0.7	5.0	5.3	3	D	2	60
3A	0.9	5.1	6.3	3	D	2	58
4B	0.9	7.0	5.2	3	P	1	52
5A	0.9	7.0	5.2	3	D+P	1	30
5B	0.9	7.0	5.2	3	D+P	1	30
3E*	1.0	5.0	5.2	3	P	1	60
2A	1.4	7.5	6.1	3	P	1	60
2B	1.4	7.1	5.6	3	D+B	2	33
3B	1.6	4.8	5.4	3	P	1	22
4C	1.6	7.0	5.2	3	P	1	57
2E*	1.6	5.0	16.9	3	P	1	43
2C	2.2	7.0	5.0	3	B+P	1	56
2D	3.8	7.0	5.2	3	P	1	43
3C	3.8	4.9	5.3	3	P	1	54
4D	5.0	5.0	5.3	3	P	1	54
4E*	10.0	6.8	5.2	3	P	1	130
1A	0.7	7.0	6.4	6	D	2	40
1B	1.2	7.1	5.9	6	D+P	2	45
5E*	1.7	5.0	16.8	6	D	2	60
1C	1.8	6.7	5.2	6	B	1	35
1E*	2.0	7.2	10.3	6	B	2	66
5C	2.2	5.4	5.5	6	B	1	73
5D	2.2	5.3	5.5	6	B	1	83
1D	2.5	5.5	6.5	6	B+P	1	60

^a * = Wide experimental cell ($W = 50$ cm); in all other cases we use $W = 15$ cm

^b D = Doming; B = Brittle; P = Plastic

258 ity. Between the sand and the clay layers, we placed a thin (~ 1 mm) layer of 0.1-0.2 mm
 259 glass beads (RETSCH), to prevent downward leaching of the fine clay into the coarse
 260 reservoir layer. To ensure that the overpressure that develops in the cell is due to gas
 261 overpressure alone, as well as to avoid hydraulic fracturing of the clay by highly pres-
 262 surized water trapped beneath the low-permeability clay, we install narrow partitions
 263 at both sides of the experimental cell. These side partitions allow the water to drain freely
 264 releasing water, while preventing gas flow and depressurization. This procedure ensures
 265 that the overpressure that develops in the cell is due to gas overpressure alone.

266 We conducted 24 individual experiments varying the thickness of clay layers (6 val-
 267 ues; note that the sand layer thickness was also varied but this parameter is not impor-
 268 tant), clay settlement duration (2 values), and cell size (2 values). The experimental set-
 269 ting as well as the emerging deformation mode and pockmark type of each experiment
 270 are summarized in Table 1, where the experimental parameters and their values are listed
 271 in Section S2 (SI). The repeatability of the experiments was verified based on two sets
 272 of runs with similar initial experimental conditions. Indeed, each set resulted in simi-
 273 lar deformation modes (4B, 5A and 5B; 5C and 5D, see Table 1). However, the specific
 274 details of the sediment deformation patterns and pressure at failure slightly differed, as
 275 expected due to unavoidable randomness in packing. We classify the PM type visually
 276 according to its geometry at the end of the experiment: (i) Type-1—regular, conical, U-
 277 shaped depressions that are empty of sediments; and (ii) Type-2—irregular depressions
 278 hosting faulted and deformed sediment.

3 Experimental results

3.1 Modes of seal breaching and gas seepage

In all experiments, we observed similar stages of gas *seepage*: (1) gas ascended through the (sand) reservoir and accumulated under the overlaying seal (clay) layer; (2) pressure progressively builds up with the continuous gas injection and accumulation, until the threshold for seal failure is met (Fig. 3); (3) the gas then seeps upwards and finally a pockmark is formed. However, the seal *failure* mode, which depends on clay layer thickness, h_c , and duration of clay settlement before injecting the gas, t_s (controlling its rigidity), differed among experiments, ranging from (i) doming, where the sealing layer bends and later breaches, allowing the escape of ascending gas through Mode I fractures; to (ii) brittle, where ascending gas pressure induced shear (Mode II) faults which served as pathways for gas escape; to (iii) plastic, where gas bubbles buoyantly rose through liquefied sediments.

Doming was the dominant mechanism in experiments where the clay was thinner and/or more rigid, and progressed according to the following stages (e.g. experiment #1A in Fig. 3 and Movies S1 and S2 in SI): (I) pressure build up in the interlayer gas pocket; (II) the overlying clay layer bends to form a dome; (III) the dome fractures by Mode I (opening) fractures and breaches; (IV) gas enters the fractures of the breached dome, widening them and seeps through; (V) The dome is deflated, causing clay blocks to collapse inward; (VI) gas continues to seep episodically through the gaps between the clay blocks, progressively disintegrating and eroding them, resulting in suspension of clay particles. Eventually, a shallow crater is created hosting collapse blocks, namely a Type-2 pockmark. In most cases, stages I–III take several minutes. Complete deflation and internal collapse of the dome (stages V–VI) require multiple gas seepage episodes. Blocks tend to interlock and can be rotated and displaced, such that a subsequent breaching of the dome and collapse requires an additional gas pressure buildup.

Brittle deformation was the dominant mechanism in experiments with intermediate thickness, rigid clay layer, and was observed to evolve in the following manner (e.g. experiment #5D, Fig. 3 and Movie S3 in SI): (I) pressure builds up to a critical point (see pressure evolution in section S1 in SI); (II) gas invades the clay layer by displacing and compressing it to create a “piston” at the base of the clay layer, in agreement with the prediction in Cathles et al. (2010). A cavity (gas bubble) starts to form within the clay, creating a mound at the top of the clay layer; (III) the gas bubble continues to grow, mostly upwards, and two sub-vertical faults appear (more noticeable at the top part of the clay), defining a free block (plug); (IV) the gas uplifts the clay block, in a piston-like motion; (V) then, gas seeps through one of the faults, along which the clay disintegrates and liquefies; (VI) with continued seepage, the plug disintegrates entirely and a U-shaped Type-1 PM forms.

Plastic deformation of the clay was dominant in experiments in which the sealing layer was relatively thick, e.g. #2D (Fig. 3) and #4E (Fig. 4), and in which the clay had less time to solidify. Deformation generally evolved in the following manner (experiment # 2D in Fig. 3 and Movies S4 and S5 in SI): similar to the case of the brittle deformation, (I) gas invaded the clay layer by displacing it to create a ‘piston’ (Fig. 4), after which (II) a bubble starts to grow within the clay at the edge of the piston (Fig. 4a), forming a mound at the top of the clay layer. Then, (III) the bubble detached from the main gas reservoir at the sand-clay boundary and migrated upwards, distorting the clay (Fig. 4a); (IV) the bubble continued to migrate upwards towards the top of the clay layer, while the clay rearranges around the bubble; (V) the bubble erupted at the top of clay layer, dragging and suspending clay particles (Fig. 4b); (VI) after a series of repeated episodes of bubble eruption a significant amount of clay was removed such that a noticeable U-shaped crater i.e. Type-1 PM formed, resembling the one formed by the plug-like brittle deformation. This stream of individual bubbles progressively weakened the

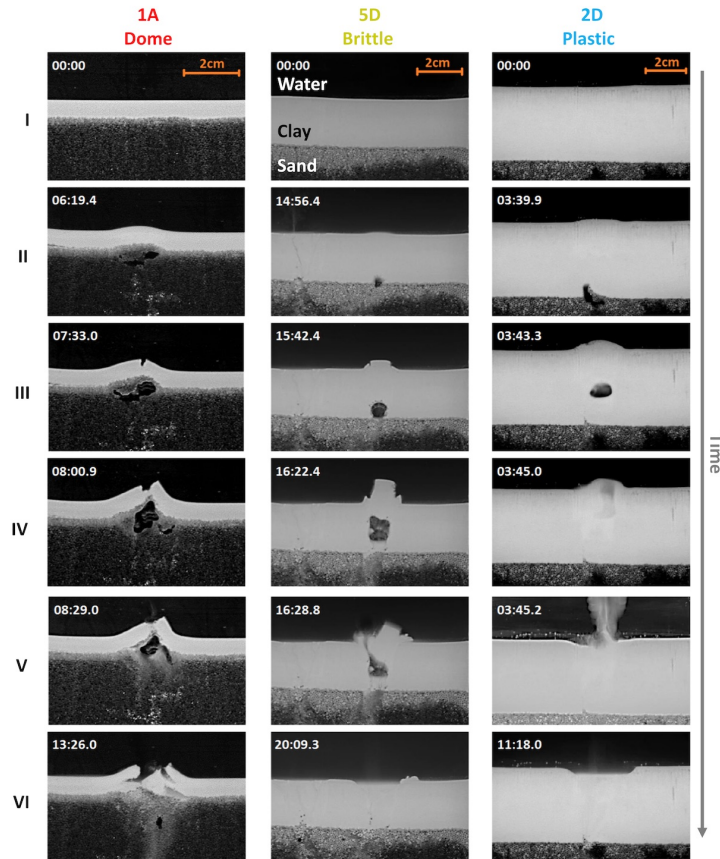


Figure 3: Snapshots showing the main stages of gas escape through a seal (gas accumulation at the seal-reservoir interface, seal breaching, gas seepage through the seal, and pockmark initiation) in three representative experiments of increasing clay layer thickness h_c (see Table 1 for details). The three experiments exemplify the three main deformation mechanism: (Left column) **Doming** (experiment #1A, $h_c = 0.7$ cm) is initiated by gas accumulation at the seal-reservoir interface. When the accumulated gas causes large enough dome deflection, the dome is breached by Mode-I (open) fracturing, leading to the development of a Type-2 pockmark (see also Movie S1 in supporting information (SI)); (Middle column) **Brittle** deformation (#5D, $h_c = 2.2$ cm). Gas accumulation at the reservoir-seal interface produces a mound in the seal, followed by Mode-II sub-vertical faulting. Seepage then occurs through these shear faults, bounding an uplifted plug, leading to the development of a Type I pockmark (see also Movie S3 in SI); (Right column) **Plastic** deformation (#2D, $h_c = 3.8$ cm), shows gas transmitted to the surface by ascending gas bubbles, leading to the development of a Type-1 pockmark (see also Movie S4 in SI). In each snapshot (only shown is the central part of the cell) the lower part (dark gray) is the top of the sand layer, and the middle part (light gray) is the clay (seal) layer which is overlaid by water (black). Rows I–VI correspond to progressive deformation stages since injection started (I); time (min:sec) since injection shown in upper left corner.

331 clay to create a damage zone (pipe) within it, serving as a conduit for further bubble mi-
 332 gration (Fig. 4C). Bubbles continuously suspend clay from the pipe such that with time
 333 the outline of the damaged pathway or pipe becomes noticeable (Fig. 4D). The migra-
 334 tion of the bubble through the clay layer (stages II–V) occurred within ~ 5 –10 s, depend-
 335 ing on the clay layer thickness (Fig. 4A–B).

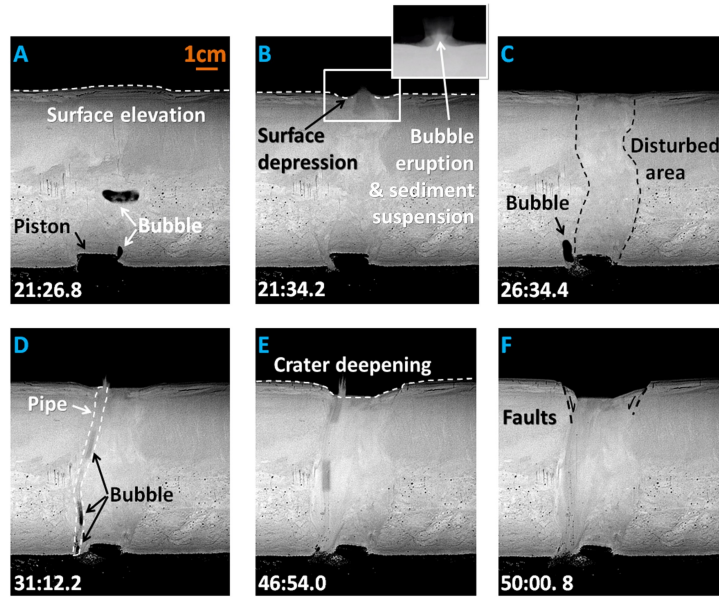


Figure 4: Experimental snapshots showing the development of a plastically-failing PM, with a feeding pipe (Experiment #4E; see Table 1 and Movie S5 in SI): (A) a piston forms with a bubble rising from its edges; (B) bubbles escape from the surface, ejecting suspended material to the water, creating a surface depression (C) bubbles initially escape from both sides of the piston, and the whole area above the piston is disturbed; (D) sequential bubble ascent creates a pipe bordering the piston; (E) episodic bubble rise through the pipe removes more material at the crater, whose borders are defined by the disturbed area; and (F) continuous development of the Type I pockmark by the collapse of the walls via faulting, interspersed by bubble escape, leading to widening of the disturbed area. The active episodes are interspersed by quiescent periods (Movie S5 in SI). Each snapshot shows the central part of the experimental cell. The lower part (black) is the top of the sand layer, and the middle part (light gray) is the clay layer which is overlaid by water (black). Time (minutes:seconds) since the start of gas flow is marked at the lower left corner of each snapshot.

336 We also observed mixed deformation modes: (a) doming/brittle deformation mode
 337 when a fault-bounded plug was developed in a dome (e.g. #2B); (b) doming/plastic de-
 338 formation when ascending gas bubbles seep through the breached dome (e.g. #5A and
 339 5B); and (c) brittle/plastic when an existing fault, serves as a conduit for packets of gas
 340 to escape as elongated (non-spherical) bubbles (#1D, cf. Fig. 5).

341 3.2 Pockmark formation and episodic seepage

342 Our experiments show that following the initial seal breaching, gas does not flow
 343 continuously upwards, unlike in ordinary percolation. Instead, flow pathway and pock-
 344 marks developed progressively during episodic seepage events. The intermittent nature
 345 of the deformation and seepage is also evident from the pressure temporal variations: gas
 346 pressure fluctuated in association with the evolution of the PM (cf. Section S1 in SI).
 347 We emphasize that the gas pressure measured in the inlet (syringe) is not associated with
 348 the gas pocket pressure after its detachment from the main gas reservoir and advance-
 349 ment into the seal layer. The evolution of PM morphology vs. number of seepage events
 350 N for each of the main deformation modes is shown in Fig. 6.

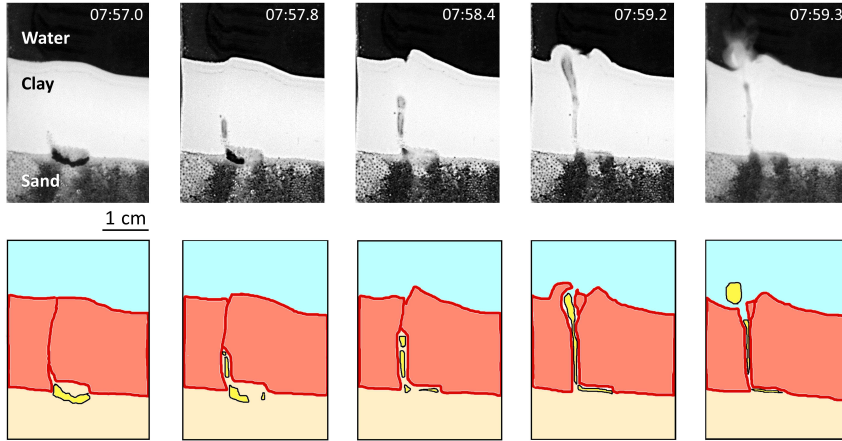


Figure 5: Experiment #1D shows a fracture and gas-filled, elongated, bubbles ascending through it. For clarity, each experimental image (top row) is accompanied by a schematic reconstructions (bottom row). The clay layer appears in white (red in the schematic), between the bottom reservoir layer in gray (yellow) and water above in black (turquoise). Bubbles appear in gray/black (yellow). Time (minutes:seconds) since the start of gas flow is marked at the upper right corner of each snapshot.

351

3.2.1 Type-2 pockmarks

352

353

354

355

356

357

358

359

360

361

In cases where the seal was initially deformed into a dome-shaped structure (that later collapsed), a complete Type-2 PM depression developed as a result of a sequential seepage through the debris of the collapsed dome (Fig. 6 #1A, $N = 7-25$). Type-2 PM seeps did not always occur from the same breach between adjacent blocks: gas was able to seep from different locations within the same PM, depending on the PM size and the number of blocks. Type-2 PMs either form from a wide dome that disintegrated into multiple blocks, or from small adjacent domes that merged into a single large PM (Fig. 6 #1B). As seepage continues, the blocks within Type-2 PMs were observed in some cases to gradually disintegrate, whereas in other cases PM morphology remained relatively unchanged.

362

3.2.2 Type-1 pockmarks

363

364

365

366

367

368

369

370

371

372

When the seal breached in a brittle or plastic manner, gas bubbles ascended through a Mode II fault or through the bulk sediment, with each seepage event deepening an erosive crater towards the development of a complete Type-1 PM. For instance, in experiments #1C and #2D in Fig. 6, the first event ($N = 1$) is seen to only slightly modify the topography, whereas seepage continued clay is progressively removed from the PM zone by its suspension into the water column, making the PM shoulders clearly evident ($N = 7$; see also Fig. 4B). Further events ($N = 7-15$) make the clay below the pockmark along the seepage route looser such that it remains in suspension, until finally ($N = 25$ in Fig. 6), most of the clay is removed all the way down to the sand layer, creating a cone-shaped Type-1 PM.

373

374

375

376

377

378

In early stages, Type-1 PMs initially deepen at a relatively uniform rate, i.e. depth D increased linearly with N (Fig. 7A), irrespective of clay layer thickness h_c . The deepening rate accelerated once $D \sim 0.2-0.3h_c$, especially for thicker clay layers. Eventually, the PM traverses the entire clay layer, $D \approx h_c$. Occasionally, PM depth decreases (Fig. 7A) due to suspended sediment or sediment from the PM rim that is falling back to the PM. The PM width L progressively increased with seepage cycles, via collapse of

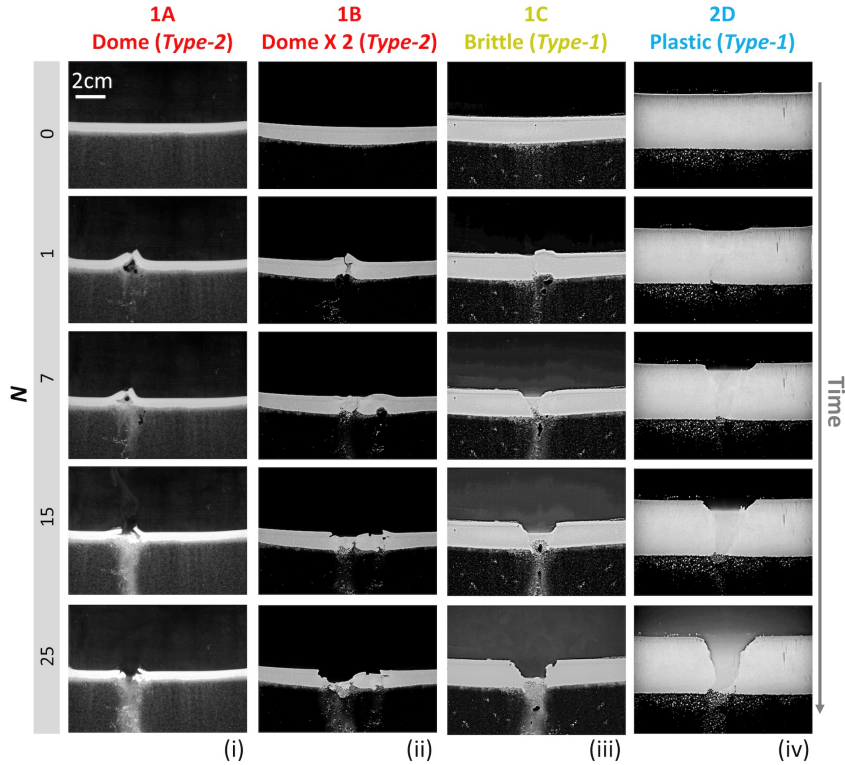


Figure 6: Experimental snapshots of pockmark development as a function of the number of seepage events, N , in four selected experiments with increasing clay thickness, h_c , exhibiting a transition in deformation mechanisms and final PM type. In each snapshot, the lower part (dark gray to black) shows the top of the sand layer, and the middle part (light gray) shows the clay (seal) layer which is overlaid by water (black). (i) Experiment #1A ($h_c = 0.7$ cm): Doming and breaching by the fracturing of the dome and development of Type-2 pockmark; (ii) #1B ($h_c = 1.2$ cm): Doming and breaching by the fracturing of a 1st dome, which is followed by the development of a second dome, its breaching and eventually development of a single Type-2 pockmark; (iii) #1C ($h_c = 1.8$ cm): Breaching by faulting, plug uplift, and development of Type-1 pockmark; (iv) #2D ($h_c = 3.8$ cm): Breaching by plastic deformation (liquefaction) around ascending gas bubble and development of Type-1 PM.

379 the PM walls (Fig. 7B; Movie S4 in SI). This collapse was episodic, that is not every seep-
 380 age event that caused widening of the PM also resulted in collapse and deepening (Fig.
 381 7C); collapse and deepening only occurred once the PM walls reached a critical angle.
 382 This is probably due to the hysteresis arising from the difference between static and dyn-
 383 amic angles of friction in granular media, i.e. in sediments (Volfson et al., 2003; Per-
 384 rin et al., 2019).

385 In many experiments, the seepage location changed with time, creating several PMs
 386 (#1B in Fig. 6 and Movie S3 in SI). The number of seepage locations was inversely pro-
 387 portional to the clay thickness, irrespective of the type of seepage mechanism and do-
 388 main size. When PMs were close to each other they merged to form a single wide PM.
 389 While our thin, quasi-2D experimental domain promotes PM merging by limiting the
 390 seepage location to a narrow line (vs. a surface in 3D domains), field observations of PM

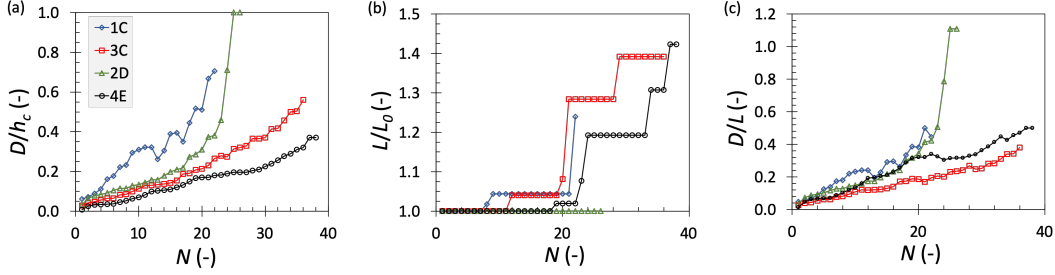


Figure 7: Quantitative analysis of the evolution of pockmark geometry vs. the number of seepage events, N , for experiments showing different deformation modes: brittle in #1C and plastic in #3C, #2D, #4E. (a) Pockmark depth, D , normalized by the clay layer thickness, h_c ; (b) Pockmark width, L , normalized by its initial value, $L_0 = L(N = 1)$; (c) Pockmark aspect ratio D/L .

391 merger (Schattner et al., 2016) suggests that this is a viable mechanism also in more com-
 392 plex, 3D domains.

393 3.3 Experimental phase diagram of pockmark formation

394 The experimentally-observed deformation mechanisms and resulting structures as
 395 a function of the clay layer properties—clay thickness, h_c , and settling time, t_s , is pre-
 396 sented as a phase diagram in Fig. 8 (see details of the experimental settings in Table 1).
 397 This diagram demonstrates the dependence of the deformation mode on the clay prop-
 398 erties: (i) **Domes** occurred only in very thin layers ($h_c < 1$ cm) in the narrower experi-
 399 mental boxes ($W = 15$ cm; used for most experiments), and at a wider range of clay thick-
 400 ness ($h_c < 2$ cm) in the wider cells ($W = 50$ cm); (ii) **Brittle deformation** was domi-
 401 nant in thicker and stiffer layers (that settled longer, $t_s = 6$ weeks); and (iii) **Plastic**
 402 **deformation** (by bubble migration) was observed in thicker, softer ($t_s = 3$ weeks) clays.

403 4 Theoretical prediction of deformation mechanisms

404 This section provides a predictive quantitative analysis of the mechanisms for seal
 405 deformation and breaching observed experimentally: doming, brittle, and plastic defor-
 406 mation. The parameters and the values used for the calculations are provided in Sec-
 407 tion S3 in the SI. In our experiments, the gas injected into the bottom of the coarse grained
 408 (reservoir) layer, rises through it and accumulates under the overlaying clay. Due to the
 409 large capillary pressure required to invade the small pores in the clay, gas remains trapped
 410 as a gas pocket, also serving as a “capillary barrier” which blocks the upwards flow of
 411 water (Morel-Seytoux, 1993). The gas overpressure driving the deformation, $\Delta P(z) =$
 412 $P_g(z) - P_w(z)$, is defined as the difference between the pressure of the gas pocket and
 413 of the water at height z , $P_g(z)$ and $P_w(z)$, respectively. In computing it, we assume hy-
 414 drostatic pressure distribution in the water column, as the side valves in our setup en-
 415 able rapid release of water pressure to maintain hydrostatic conditions (Fig. 2). We stress
 416 that, even in a fully hydrostatically balanced system, buoyancy forces can create over-
 417 pressure (Osborne & Swarbrick, 1997). To illustrate this, consider a gas pocket of height
 418 h_g disconnected from the syringe (Fig. 2). At the base of the gas pocket, the gas pres-
 419 sure is equal to that in water-saturated (gas-free) regions at a similar depth. Inside the
 420 gas pocket, the pressure decreases with elevation as $-\rho_g g h_g$, i.e. more gradually than
 421 in the water phase (P_w decreases as $-\rho_w g h_g$), where ρ_w and ρ_g are the density of wa-
 422 ter and gas respectively, and g is the gravitational acceleration. This implies that the
 423 gas overpressure at the bottom of the clay is proportional to the height of the gas pocket,

424 $\Delta P = (\rho_w - \rho_g)gh_g$. As the volume of the trapped gas pocket increases and h_g grows,
 425 ΔP at the top of the pocket increases until it suffices to deform the seal. It is possible
 426 that in our experiments there was a connected gas pathway from the syringe to the base
 427 of the seal; this could not be deduced from image analysis. In such a case, gas overpres-
 428 sure would exceed that arising from buoyancy (hydrostatic) forces alone.

429 The stress in the clay is computed assuming lithostatic distribution, i.e. that the
 430 clay grains support their own weight plus the weight of the water, $\sigma_{v,lit} = \rho_c h_c g + \rho_w h_w g$,
 431 where ρ_c is the saturated clay density, h_c is the clay thickness, and h_w is the water depth
 432 from the surface to the top of the clay layer (Fig. 2). Thus, the effective stress at the bot-

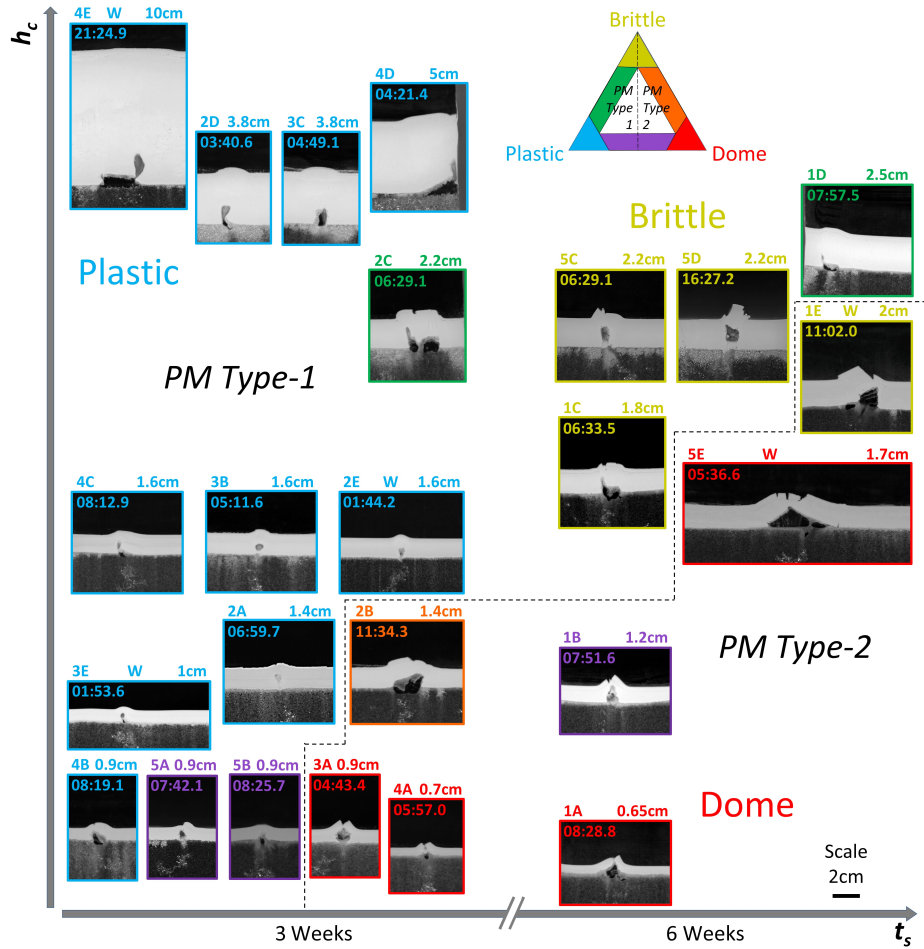


Figure 8: Experimental phase diagram of deformation mechanisms vs. settings in terms of clay thickness, h_c , and settling time, t_s . Final pockmark geometry is shown for 14 experiments, including (top row) the experiment number (left), “W” if the wider (50 cm) cell was used, h_c (right), and the time elapsed since seepage initiation (hh:min), below. The diagram is divided into PM Type-2 domain and Type-1 domain, where the boundary is marked by a dashed line. The axes are not up to scale, i.e. snapshot locations are relative: higher indicates larger h_c , and left and right correspond to t_s is 3 or 6 weeks, respectively. Snapshots are color-coded by formation mechanism (see the phase triangle): doming (in red); brittle plug development and seepage through fractures (yellow); plastic deformation by bubbles (blue); mixed doming/plastic mode (purple); mixed doming/brittle (orange); mixed brittle/plastic (green).

433 tom of the saturated clay layer is

$$\sigma'_v = (\rho_c - \rho_w)h_c g. \quad (1)$$

434 Clay deformation in our experiments occurs much faster relative to the flow and pres-
 435 sure relaxation of water in the clay, such that we consider undrained conditions (in con-
 436 trast to the assumption in Cathles et al. (2010)). This can be justified by scaling: we ob-
 437 serve clay deformation within seconds—the time for a bubble to traverse the clay layer
 438 by deforming it (e.g. see fig. 3, right column). The timescale for the flow across the layer
 439 can be evaluated from Darcy’s law. We note that clay permeability can span a large range,
 440 10^{-20} – 10^{-14} m², (Chapuis & Aubertin, 2003; Neuzil, 1994); using the higher value of
 441 10^{-14} m² provides the lower bound for the flow timescale. The gas pressure difference
 442 between the bottom and the top of the clay was not measured; we use instead the upper
 443 bound for gas pressure in the experiments, ~ 2 kPa (Fig. S1 in SI). Assuming poros-
 444 ity of 0.1 and $h_c = 10$ cm, provides an upper limit of ~ 1 μ m/s for the velocity of wa-
 445 ter drainage from the clay, corresponding to $\sim 10^5$ s (across a distance of $h_c = 10$ cm),
 446 orders of magnitude longer than the time of deformation. This justifies our undrained
 447 assumption.

448 In the Sections below, we derive theoretical expressions for the conditions required
 449 for each mode of clay deformation, relying on the ”critical state soil mechanics” theory
 450 (Wood, 1991). Details and parameter values are provided in Section S2 in the SI.

451 4.1 Dome breached by fracturing

452 Consider an elastic dome, breached by a fracture when deflection becomes large enough
 453 (as in experiments # 1A, 5E, 4A, 3A in Fig. 8). The conditions for this mechanism are
 454 evaluated using analytical expressions from the three-point beam flexure theory (Bower,

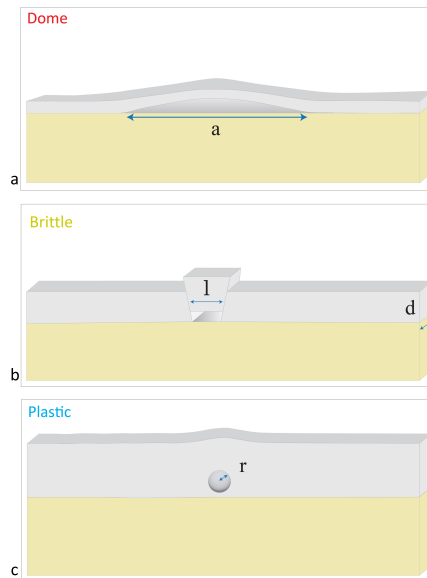


Figure 9: Characteristic length scales used in the analysis of the different seal breaching and deformation modes: (a) gas pocket forming a dome (dome width: a); (b) faults creating a plug (of base length l and thickness d), lifted by a gas pocket; (c) gas bubble (of radius r) rising within the clay.

2009). This theory computes the deformation of a rectangular beam loaded at its middle while supported at its edges. Beam failure occurs when the strain at its outer (curved) edge exceeds its tensional strength. This scenario is used as an approximation for our quasi-2D experiments, where the gas pushes the clay seal from below approximately at its centre (experiment #1A in Fig. 3, and # 1E, 5E in Fig. 8). The pressure required to fracture in tension a beam (dome) of length a (Fig. 9a) by a pressure ΔP_{dome} is (Bower, 2009)

$$\Delta P_{\text{dome}} = \frac{2}{3} \frac{h_c^2 (\sigma'_v + T_0)}{W a} \quad (2)$$

where T_0 is the clay tensional strength and W is the cell width.

4.2 Brittle deformation

Brittle failure occurs in our experiments via formation of a a block bordered by faults ("plug"), e.g. see experiment # 5D in Fig. 3 and #1E, 1C, 5C in Fig. 8. The first step in creating a plug is by forming a gas "piston" (see elaborated discussion in Section 4.3.1). In brittle layers, upward piston motion produces sub-vertical side faults that delineate the plug. The plug is then lifted by frictional sliding along the faults (#1A, 1C, 5C in Fig. 8). The fractures surrounding the plug—which is often tilted—act as gas escape pathways.

The gas overpressure required to induce faulting that creates and lifts a plug, ΔP_{plug} , must overcome two forces: one to create faulting in the clay layer, F_{frac} , and another to slide the plug upwards on the 2 faults delineating it, F_{slid} .

$$\Delta P_{\text{plug}} = \max(F_{\text{frac}}, F_{\text{slid}}) / A_b. \quad (3)$$

Here $A_b = dl$ is the area of the plug base, d is the spacing between the plexiglass walls, and l is plug length (Fig 9B). The shear force required to create a fault is related to the gas pressure via $F_{\text{frac}} = A_b \Delta P_{\text{frac}}$, which in turn can be obtained from the criterion for fracturing of clay by shear (Marchi et al., 2014),

$$\Delta P_{\text{frac}} = \sigma'_3 + n c_u = \sigma'_v + n c_u. \quad (4)$$

Here n is an empirical coefficient of order unity (Atkinson et al., 1994). In Eq. (4) and the calculations hereafter, we assume $\sigma'_3 \approx \sigma'_v$. The undrained shear strength of clay is (Eq. 8 in Mayne (2001))

$$c_u = 0.5 \sigma'_v \sin(\phi) (OCR)^\gamma, \quad (5)$$

where ϕ is the undrained friction angle, OCR is the overconsolidation ratio, and σ'_v is the effective stress, given by Eq. 1 for clay seal base. The exponent γ is found empirically (Z. Sun & Santamarina, 2019). For the selection of parameter values, including ϕ , n , γ and OCR , see section S2 and Table 2 in SI.

The sliding force F_{slid} in Eq. 3 is computed as the sum of the following forces: (i) frictional resistance to the sliding of the plug against its two bordering faults (assumed to be sub-vertical), $2\sigma'_v \mu_c h_c d$; (ii) frictional resistance with the cell walls, $2\sigma'_v \mu_w h_c l$; and (iii) the force to lift the plug weight, $\sigma'_v A_b$:

$$F_{\text{slid}} = \sigma'_v (2\mu_w h_c l + 2\mu_c h_c d + dl) \quad (6)$$

where μ_c and μ_w are the clay-clay and clay-wall friction coefficients, respectively (see Section S2 in the SI). Substituting F_{frac} and F_{slid} into Eq. 3 provides the critical pressure for brittle deformation,

$$\Delta P_{\text{plug}} = \max \left[\sigma'_v + n c_u, \sigma'_v \left(2\mu_w \frac{h_c}{d} + 2\mu_c \frac{h_c}{l} + 1 \right) \right]. \quad (7)$$

492

4.3 Plastic deformation

493

494

495

496

497

498

The third possible mode of seal failure is the creation of a cavity by plastic deformation (9C). This cavity may form by the rise of either a “piston” or a gas bubble (Fig. 4A). In thin clays (#4C, 2E, 3B in Fig. 8) bubbles are created at the bottom or middle of the clay layer. In thicker clays bubbles are often generated from tips of a flat piston (Cathles et al., 2010) that first yields into the clay (Fig. 4; Fig 8 #4C, 4D). The conditions for the different stages of plastic deformation are computed below.

499

4.3.1 Piston formation

500

501

502

503

504

505

506

507

508

509

510

511

In some of the experiments with thick seals, a “piston” developed above the large gas pocket pushing into the clay seal. The piston, shaped by the capillary forces associated with interfacial tension, has a relatively flat top and limited width. Cathles et al. (2010) hypothesized (i) the development of such a piston; (ii) that the piston dimensions depend on the pore size distribution; and (iii) the rising piston will liquefy the sediments above it, allowing it to accelerate upwards. Our experiments indeed demonstrate that in some cases a piston is created, and our calculations below predict that it will liquefy the clay above it. However, we do not observe an acceleration of the piston; instead, we observe that the piston comes to a halt, and the trapped gas escapes via bubbles emanating from its edges (Fig. 4). Bubble formation at the edges is aided by stress concentration at the sharp edges of the piston. The conditions for this mechanism are quantified below.

512

4.3.2 Bubble and cavity formation

513

The pressure required to form a gas-filled cavity (bubble or piston) in the clay is

$$\Delta P_{\text{cavity}} = \sigma'_v + 1.3c_u \left[1 + \ln \left(\frac{E}{2c_u(1 + \nu)} \right) \right], \quad (8)$$

514

515

516

517

518

519

520

521

where E and ν are Young’s modulus and Poisson ratio of the clay (Z. Sun & Santamarina, 2019). Eq. 8 implies that ΔP_{cavity} always exceeds the liquefaction threshold, $\sigma'_v + c_u$, supporting the hypothesis that clay will be liquefied around the cavity. Liquefaction allowing bubbles to ascend by pushing the clay in front of them was observed experimentally by Varas et al. (2011); Ramos et al. (2015). Furthermore, as both σ'_v and c_u are proportional to clay thickness h_c (Eqs. 1, 5), Eq. 8 suggests a that the pressure of the bubble or piston also increases with h_c , as confirmed by our experimental data (Fig. S2 in the SI).

522

4.3.3 Bubble ascent

523

524

525

526

527

A gas bubble will continuously grow in place until the buoyancy force overcomes the drag force, allowing it to ascend (Fig. 10). Bubble ascent requires an additional force (beyond that required for bubble formation and liquefaction) to overcome the drag force resisting the bubble motion within the clay. The drag force is estimated here via dimensional analysis,

$$F_d = kc_u\pi r^2, \quad (9)$$

528

529

530

where r is bubble radius and k is an empirical parameter. The buoyancy force acting to lift the bubble is computed from the weight of the submerged clay it displaced, of volume similar to that of the bubble, $4/3\pi r^3$:

$$F_b = (\rho_c - \rho_w) \frac{4}{3} \pi r^3. \quad (10)$$

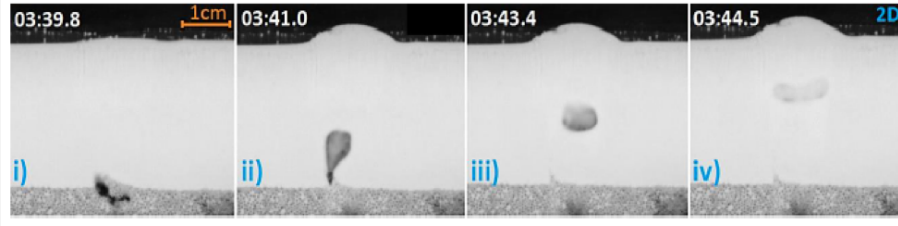


Figure 10: Four stages of bubble migration in clay (experiment #2D): (i) Gas invasion, (ii) bubble vertical growth and detachment, (iii) rounded bubble migration, (iv) bubble flattening due to its movement upwards. In each snapshot, the lower part (dark gray) shows the top of the sand layer, and the middle part (light gray) shows the clay (seal) layer which is overlaid by water (black). The time elapsed since seepage initiation (hh:mm) appears in the upper left corner.

531 Once the bubble reaches a critical radius, $F_b = F_d$, and it starts to rise. The critical
 532 bubble radius to overcome the drag is computed from the above together with Eq. 5,

$$r_c = \frac{3kc_u}{4(\rho_c - \rho_w)} = 0.13kgh_c(OCR)^\gamma. \quad (11)$$

533 Eq. 11 predicts a dependence between the critical bubble size and layer thickness h_c , in
 534 agreement with our experimental observations (Fig. S2 in SI). We note that Eq. 11 re-
 535 lies on the assumption of a spherical bubble, whereas in many cases bubbles were dis-
 536 torted during ascent, e.g. see Figs. 5 and 10. This, together with the limited number of
 537 experimental data points, prevented a reliable estimate of k from our data.

538 4.3.4 Pipe and pockmark formation by bubble ascent

539 Bubbles ascend while liquefying the sediment in front of them. This leaves a record
 540 of the gas passage in the form of a liquefied pathway within the clay (Fig. 4), provid-
 541 ing an easier pathway for subsequent bubble ascent (by reducing both ϕ and OCR , and
 542 hence c_u , cf. Eq. 5). Repeated occurrence of this mechanism creates a localized gas pipe
 543 (Fig. 4D, E), of a width that is correlated with the bubble dimensions. Each escaping
 544 bubble also deepens the crater (Fig. 4E and Fig 7a). As the crater walls repeatedly col-
 545 lapse by faulting and sliding (Fig. 7b), it forms a pockmark (Fig. 4F) of increasingly larger
 546 depth to width ratio (Fig. 7c). In some cases when fractures form, they serve as pipes
 547 for venting elongated bubbles (that fit the fracture width, cf. #1D in Fig. 5), a mixed
 548 brittle/plastic deformation mode (e.g. #2C in Fig. 8).

549 4.4 Transition between failure mechanisms

550 Following a gas pocket buildup at the base of the clay seal, gas escapes in our ex-
 551 periments by either (i) fracturing an elastic dome; (ii) brittle deformation, as a plug de-
 552 lined by faulting; or (iii) plastically, by ascending bubbles. The dominant failure mech-
 553 anism is the one requiring the least gas overpressure (e.g. Z. Sun & Santamarina, 2019),
 554 which we compute from Eqs. 2, 7 and 8. This dominant overpressure and the correspond-
 555 ing mechanism is shown in Fig. 11(a–b) for two clay consolidation states, $OCR = 0.5$
 556 (a; representing short settling time of $t_s = 3$ weeks) and $OCR = 1$ (b; $t_s = 6$ weeks). These
 557 low OCR values are representative of the loose state of our system, which compacted
 558 under its own weight only. As expected, the failure pressure mostly increases with in-
 559 creasing clay thickness h_c . For loosely compacted clays (Fig. 11a), the mode of preferred
 560 failure transitions from dome to bubble at $h_c \simeq 1$ cm. For stiffer, more consolidated

561 layers (Fig. 11b), the mode of failure transitions from doming to brittle faulting at $h_c \simeq$
 562 0.7cm , and from faulting to bubbles (plastic) at $h_c \simeq 2\text{cm}$.

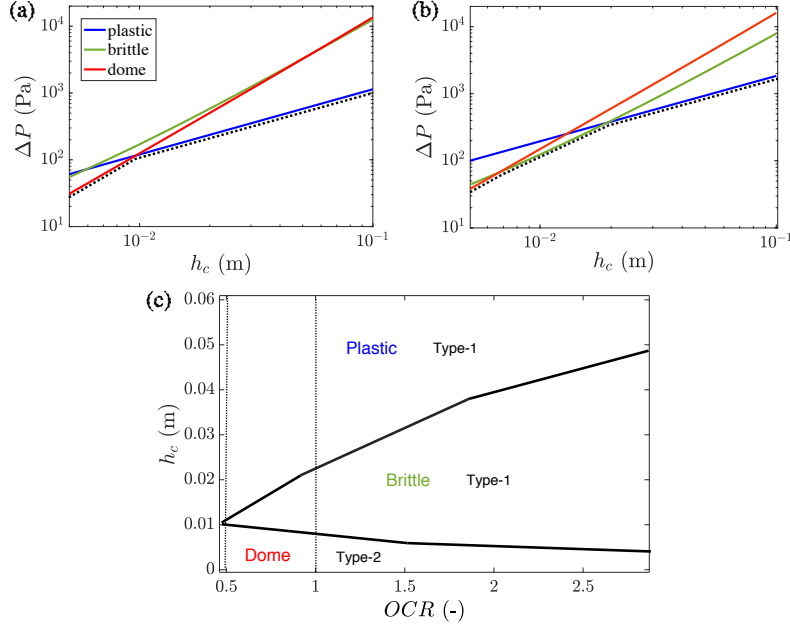


Figure 11: Calculated gas overpressure required to activate each of the 3 failure modes of the seal in our experiments (solid lines; Eq. 2 in red, Eq. 7 in green, and Eq. 8 in blue), and expected PM types, as function of clay layer thickness h_c , for two different representative consolidation degrees: (a) $OCR=0.5$; and (b) $OCR=1$. The dominant deformation mode is set by the mechanism requiring the minimal value of ΔP (dotted black lines). (c) Theoretical phase diagram for the preferred (minimal ΔP) deformation mode, as function of clay layer thickness and OCR value, adding more OCR values in addition to those shown in (a) and (b).

563 A phase diagram showing the expected mode of failure as a function of OCR and
 564 clay thickness h_c is presented in Fig. 11c. Values of $OCR > 1$ are of practical interest
 565 as in nature there are larger stresses that produce greater consolidation. Fig. 11c shows
 566 that domes are predicted to be the preferred deformation mode for very thin layers (here
 567 $h_c < 1$ cm). For thicker layers, the mode of failure transitions with increasing h_c , first
 568 to brittle faulting creating a plug, and then to plastic: for soft clay ($OCR = 0.5$), lay-
 569 ers thicker than 1 cm will degas by bubbles. In more rigid clays ($OCR = 1$) layers of
 570 intermediate thickness (here $1 \leq h_c \leq 2.25$ cm) will degas by lifting a faulted plug,
 571 while clays with $h_c > 2.25$ cm will still degas by bubbles. As the clay compacts more
 572 (larger OCR), the transition from brittle to plastic occurs at increasingly larger h_c .

573 5 Discussion

574 5.1 Theory of seal deformation applied to experimental results

575 Our experiments show that the mode of deformation controls the eventual PM type:
 576 Domes lead to Type-2 PM while brittle and plastic deformation create a Type-1 PM;
 577 e.g. see Fig. 6 and 8. Our analysis (Fig. 11c) suggests that the mode of deformation and
 578 thus the eventual PM type co-depend on two experimental parameters: clay thickness
 579 h_c and settling time t_s . The time t_s controls the degree of consolidation (as measured

580 by the *OCR*), thus affecting the clay elastic modulus (Eq. S2 in SI) and shear strength
 581 c_u (Eq. 5). t_s also affects the tensile strength, T_0 (Eq 2). Seal thickness h_c also affects
 582 all modes of failure, appearing directly or indirectly in all failure conditions (Eqs. 2, 3
 583 and 8). In this way both h_c and t_s affect the strength for dome breach, and brittle and
 584 plastic failure. The theoretical phase diagram (Fig 11c) is in general in good agreement
 585 with the experimental data (phase diagram in Fig. 8). Both the experiments and the
 586 theory suggest that doming would dominate for the thinnest layers, plastic deformation
 587 by bubble ascent for the thickest layers, and brittle faulting more dominant for interme-
 588 diate layer thickness, with faulting in stiffer, more settled layers. A corresponding tran-
 589 sition from Type-2 to Type-1 PM is seen experimentally and predicted theoretically. The
 590 experiments also support the theoretical prediction that the critical clay thickness (h_c)
 591 value at the transition between Type-2 to Type-1 PM increases with the system size (width
 592 of the experimental cell); e.g. in Fig 8 experiment #5E (wider cell) is deformed by dom-
 593 ing whereas #1C (narrower cell, nearly identical h_c) produces faulting.

594 Despite the overall agreement between our experimental data and theory, the the-
 595 oretical critical pressure in Fig. 11(a–b) cannot be directly validated by our experiments.
 596 This is because once the gas pocket detaches from the inlet (syringe) and ascends (see
 597 e.g. Movie S1 in SI), its pressure is no longer associated with that of the reservoir (in-
 598 let, where we measure the pressure, cf. Fig. S1 in SI). Instead, we could estimate bounds:
 599 the inlet pressure provides an upper bound, whereas $(\rho_w - \rho_g)gh_g$ provides a lower bound
 600 , where h_g is the height of the detached gas pocket. The theoretical values in Fig. 11(a–
 601 b), ~ 100 - 1000 MPa, are well within the bounds evaluated from our experiments.

602 5.2 Theory of seal deformation applied to field conditions

603 The application of the theoretically predicted deformation mechanisms to field condi-
 604 tions and scales requires (i) extending the calculations from 2D to 3D; (ii) consider-
 605 ing thicker seal layers, i.e. h_c of 1–1000 m (Koch et al., 2015; Moss & Cartwright, 2010);
 606 and (iii) higher stresses. The expressions predicting the critical overpressure correspond-
 607 ing to each deformation mode are provided below, and plotted vs. clay thickness h_c in
 608 Fig. 12.

609 **Doming** in 3D corresponds to an overpressure of (Barry et al., 2012; Koch et al.,
 610 2015),

$$\Delta P_{dome3D} = \frac{8}{3} \frac{E}{1-\nu} \frac{h_c w_{max}}{a^4} \left(\frac{2h_c^2}{1+\nu} + w_{max}^2 \right) + \sigma'_v \quad (12)$$

611 where w_{max} is the dome maximum vertical deflection, and a is its lateral dimension. To
 612 compute the pressure in Eq. 12 we use the parameter values for a/h_c , w_{max}/a and E from
 613 (Koch et al., 2015), as discussed in Section S3 in the SI. We note that this computation
 614 is poorly constrained by field observations due to the large uncertainty (wide bounds)
 615 in the values of the governing parameters a , w_{max} (Barry et al., 2012) and E (Koch et
 616 al., 2015). In addition, doming does not imply the mode of seal breaching, and there-
 617 fore the above does not provide a critical overpressure for seepage.

618 **Brittle deformation** due to overpressure in field settings will either involve open-
 619 ing (Mode I failure) of pre-existing faults or fractures, or the creation of new faults (hy-
 620 drofractures), through which gas will seep. "Plug-lifting" along faults, observed in some
 621 of our experiments, is not expected to occur in the field, as it is due to the small dimen-
 622 sion of our experimental cell and our 2D settings. To lift a plug requires that the force
 623 exerted by the gas overpressure, exceeds the weight of the plug plus friction force on all
 624 four surfaces bounding the plug. Yet, these forces (stress times area) increase with sys-
 625 tem scale. Transmitting gas via an opening-mode pulse (i.e., rising penny-shaped bub-
 626 bles (Boudreau et al., 2005)) only require stress to locally exceed a threshold. Thus, gas
 627 transmission through field-scale faults is expected to occur in rising disk-like bubbles,
 628 as observed in the gas-injection-into-gelatin experiments of (Boudreau et al., 2005; Boudreau,

2012), and also in some of our thick-seal experiments, e.g. Fig. 5. To open a pre-existing fracture the gas overpressure must exceed the effective confining stress, whereas to form and open a new hydrofracture requires an even higher overpressure (cf. Eq. 4), see Fig. 12.

A bubble can rise buoyantly in fractures once its buoyancy force exceeds the drag force, where the critical bubble size depends on its shape and size, and on layer thickness (Section 4.3.3). Extending our computations relying on the assumption of a spherical bubble (Eq. 11) is beyond the scope of this paper.

Note that once one gas bubble ascends through a fault or fracture it decompacts the sediment in its pathway, locally reducing its strength (Eq. 5), which in turn favors future gas ascent within this route, localizing it into a gas pipe.

Plastic deformation by bubbles forming in intact sediment (without fracturing) in the field is expected to require the same overpressure as in the experiments (Eq. 8), see Fig. 12 (blue line).

Capillary invasion was not discussed in relation to our experiments, due to the prohibitively high capillary entry pressures in the fine clay we used as seal. The gas overpressure required to push it into water-filled pore throats of size r is

$$\Delta P_{\text{cap}} = \frac{2\gamma_{gw}}{r} \quad (13)$$

where γ_{gw} is gas-water surface tension (0.072 N/m). The pore sizes in natural clays span a wide range which is hard to constrain. Fig. 12 shows an estimate for intact shale, assuming for simplicity a constant r with depth. As a rough estimate, we use the dominant pore size $r \sim 0.03\mu\text{m}$ measured in unconfined shale (Makhnenko et al., 2017), providing an overpressure of $\Delta P_{\text{cap}} \sim 4.8$ MPa (horizontal dashed line in Fig 12). If r decreases with confinement (depth) ΔP_{cap} will grow.

The mode of sediment failure which will be preferred is the one requiring the least pressure. Our theoretical analysis (Fig. 12) suggests that doming will constitute the initial stage of many PMs; this agrees with the common interpretation of field-observed domes (A. Judd & Hovland, 2009; Barry et al., 2012; Koch et al., 2015). However, doming as early stage deformation model does not in itself imply the dominant mode during further seal breaching and gas seepage. Following initial doming, our theoretical analysis (Fig. 12) predicts gas escape by opening pre-existing faults and fractures (as seen experimentally, cf. Fig 5). Without pre-existing faults, hydro-fracturing is expected to occur, at slightly higher over-pressure. In domes, the overpressure required to fracture/fault the dome will be lowered relative to those required to fracture a flat seal, due to the extensional fiber stresses exerted by the dome flexure (for calculation of these stresses see Turcotte and Schubert (2014), section 3.12), but we do not further pursue this calculation due to the very variable elastic modulus value.

Following conduit opening, gas bubbles will rise once reaching a critical radius, set by layer thickness and bubble geometry, leaving an elongated weakened pipe-like structure behind. We do not expect bubbles to rise freely in *undisturbed* sediment, due to the large pressure required, which is much higher than that to create a hydrofracture.

Once bubbles, rising in faults or fractures, reach the seal surface, they may create a PM via "erosive fluidization" (Cartwright & Santamarina, 2015): gas eruption ejects sediments to the shoulder of a PM, eroding the surface and creating a depression (e.g. Figs 5 and 4). This PM formation process constitutes a combination of several different mechanisms for gas transport to the surface which were discussed earlier. We emphasize that our experiments indicate that fluidization and associated erosion do not require a fluid jet (as suggested by Cartwright and Santamarina (2015)).

675 **5.3 Implications from tabletop experiments and theory to natural pock-**
 676 **marks**

677 Our experiments uniquely observe the entire process of gas seepage from the reser-
 678 voir to the surface (sea floor), i.e. the initial pressure-induced seal failure followed by the
 679 passage of gas through the seal, and finally the formation of PMs at the surface, where
 680 gas seeps out (Fig. 6). The deformation mechanisms forming the PMs differ between ex-
 681 perimental and field conditions: In experiments either brittle failure or ascent of rela-
 682 tively spherical bubbles in liquefied clay can occur (depending on experimental setting),
 683 whereas in the field brittle deformation is expected to dominate, with elongated bubbles
 684 rising through fractures or faults. The observations in the field regarding the role of fault-
 685 ing are equivocal: while some (e.g. Crutchley et al. (2021)) suggest that gas preferen-
 686 tially rises through vertical fractures instead of through pre-existing faults, others show
 687 that pre-existing faults control gas escape (Hustoft et al., 2009). The mechanisms of seal
 688 breaching and bubble ascent (Fig. 3) control not only the manner by which the gas seeps
 689 out to the surface but also the sediment suspension in the water column, the episodic
 690 nature of the seepage, and the eventual PM shape (Fig. 6). Below we compare our find-
 691 ings to field observations.

692 **5.3.1 Gas migration through the sediment**

693 Based on analysis of fluid escape pipes morphology and their geological context us-
 694 ing seismic sections, Løseth et al. (2011) and Cartwright and Santamarina (2015) con-
 695 cluded that pipes play a critical role in providing leakage pathways for trapped hydro-
 696 carbons through overlying seals. Løseth et al. (2011) suggested hydro-fracturing of the
 697 seal as the main mechanism for breaching and pipe formation. In contrast, Cartwright

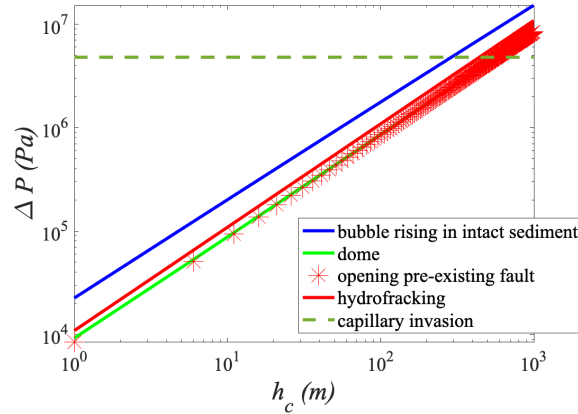


Figure 12: Calculated overpressure required to initiate deformation under field condi-
 tions. Doming (solid green line; Eq. 12) and opening of existing faults and fractures (red
 stars; $\Delta P = \sigma'_v$) require nearly the same overpressure, and are the 2 favored deformation
 modes. Hydrofracking, i.e. opening new fractures, requires only slightly higher overpres-
 sure (solid red line; Eq. 4). Gas Bubbles rising freely in the sediment (blue line; Eq. 8)
 are unlikely since they require much higher pressure than the brittle modes. Ignoring
 compaction, capillary invasion pressure is constant with depth (horizontal dashed line;
 Eq. 13). This phase diagram predicts that (until at least 1km depth) gas overpressure will
 create domes and escape by bubbles opening pre-existing fractures, if such exist. Oth-
 erwise, domes will form, followed by hydrofracking and gas ascent in bubbles through
 them.

698 and Santamarina (2015) excluded over-pressurized fluid related processes (such as hy-
 699 draulic fracturing, erosional fluidization and capillary invasions) as the dominant mech-
 700 anism forming pipes; instead, Cartwright and Santamarina (2015) suggested localized
 701 collapse due to volume loss and syn-sedimentary flow localization as possible mechanisms
 702 for pipe growth, where initiation might be controlled by the above over-pressurized fluid
 703 related mechanism. Our experiments support a combination of the processes suggested
 704 by Cartwright and Santamarina (2015) and Løseth et al. (2011). In our experiments we
 705 observe that during the initial stage escape features (bubbles, faults, domes) form by high
 706 pore pressure. After the initial weakened zone forms, pipes develop as disrupted zones
 707 by repeated material degradation (Figs. 3, 4). Pipes direct gas seepage from the reser-
 708 voir, through the seal to the seafloor (Fig. 4), in agreement with field data in Løseth et
 709 al. (2011) showing pipes traversing throughout the seal all the way to the seafloor. Our
 710 experimental observations also agree with the model suggested by Løseth et al. (2011):
 711 overpressure buildup and release via pipes, and the formation of a mound at the pipe
 712 upper terminus, resulting in ejection of fluidized sediment close to the surface (rather
 713 than from depth). Our experiments also agree with the common hypothesis (Cartwright
 714 and Santamarina (2015) and elsewhere) relating the termination of pipes at the seafloor
 715 to PMs.

716 Another finding in our experiments that is relevant to field conditions is our obser-
 717 vation of a mixed seepage mechanism, in which bubble pulses rise along brittle frac-
 718 tures (Fig. 5). Like the vertical gas pipes, the fractures or faults become liquefied pipes
 719 after bubbles traverse them, promoting transport of further bubble trains in these pipes.
 720 Our theoretical analysis indicates that this gas-escape mode would be ubiquitous in na-
 721 ture, in agreement with Z. Sun and Santamarina (2019). This theoretical prediction is
 722 supported by field data in the form of seismic micro-events in soft sediments, attributed
 723 to bubble rise and escape via faults (Tary et al., 2012).

724 In terms of bubble geometry, our experiments show that the rising bubbles are flat-
 725 tened into disk shapes (Fig. 5), similar to the reports in natural sediments by Marcon
 726 et al. (2021), and to the Boudreau et al. (2005) experiments of gas injection into gelatin.
 727 Furthermore, bubble disk radii were seen in our experiments to correlate with pipe widths,
 728 as seen in Figs. 4D and 5 (Note that the final localized pipe width may be much nar-
 729 rower than the initially disturbed zone width, as shown in Fig 4D). Thus, pipe widths
 730 are expected to grow with bubble radii, which in turn increase with seal layer thickness
 731 (experimental observation showing increasing of bubble radius with clay thickness are
 732 presented in Fig. S2 in SI). Hence, we expect the experimentally-observed \sim cm-scale pipes
 733 to scale up to 10-100 m in natural sediments, as observed in the field (Cartwright & San-
 734 tamarina, 2015; Crutchley et al., 2021). The elongated bubble shape implies that bub-
 735 ble rise can happen at lower bubble volumes than that predicted by Eq. 11, as the drag
 736 force which resists the bubble migration is proportional to the cross-section in the di-
 737 rection of motion. As the confinement imposed by lithostatic stress reduces with the bub-
 738 ble height within the sediment, near the sediment surface the bubbles may resume their
 739 spherical shapes (Z. Sun & Santamarina, 2019).

740 **5.3.2 Pockmark geometry**

741 Our experimental observation of a transition from Type 2 to Type 1 PMs as seal
 742 thickness, h_c , increases, also correlates with deepening of PMs, i.e. experimental Type
 743 2 PMs are generally shallower (smaller PM depth, D) than Type 1 PMs. This agrees with
 744 trends observed in the field, where D also increases with h_c (e.g. Fig 10 of Brothers et
 745 al., 2012) and Type 2 PMs are often observed to be shallower than Type 1 PMs (Riboulot
 746 et al., 2016). We speculate that the transition between the PM types may arise from frac-
 747 ture spacing: layer thickness controls fracture spacing (Wu & Pollard, 1995), and thus
 748 thin layers will break into smaller blocks delineated by more closely-spaced fractures, which
 749 in turn would favor creation of the complex, Type 2 PMs (e.g. experiment #1B in Fig.

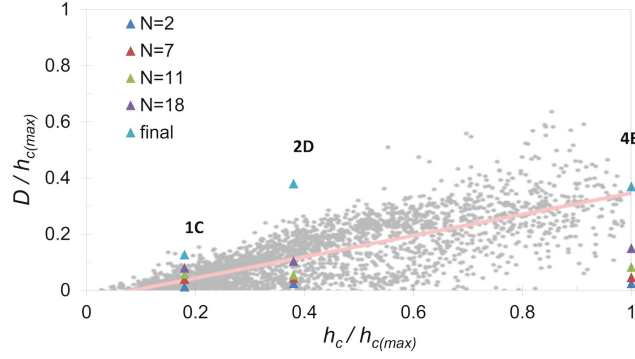


Figure 13: Comparing the pockmark depth D against clay thickness h_c between our experiments (triangles) and field observations (gray dots). To compare between the laboratory and field scale, we normalize both D and h_c by the maximal thickness $h_{c(max)}$. The value of $h_{c(max)}$ was 45 m for the field data, and 0.1 m for experiments (the value obtained in #4E). Also shown is the evolution of $D/h_{c(max)}$ with number of seepage events N (legend) for the 3 presented experiments: #1C (brittle), # 2D and # 4E (both plastic deformation); see also Fig. 7. Field data is from 3066 pockmarks offshore Maine, US (modified from Brothers et al. (2012)); the pink line shows a linear trend for this population ($R^2 = 0.60$).)

750 6). In contrast, large fracture spacing in thick layers would favor creation of simpler Type-
 751 1 PM with seepage from only a few, widely-spaced fractures. Another feature we observed
 752 experimentally, which was also observed in the field, is that Type I PMs retain a rela-
 753 tively equidimensional depression shape (Fig. 5), despite the rise of elongated bubbled,
 754 as seen by Crutchley et al. (2021); Hsu et al. (2021); Marcon et al. (2021). However, in
 755 cases where doming collapse led to clay breaching, seepage from multiple points between
 756 semi-rigid clay blocks resulted in Type-2 pockmarks with uneven depression (Figs. 6, 8).

757 Our observation of increasing pockmark depth D with time, until it traverses the
 758 entire clay layer (i.e. approaching the clay thickness h_c) (#2D in Fig. 6), is in general
 759 agreement with field observations, e.g. Andresen et al. (2021), which relates PM deep-
 760 ening to gas seepage events, as a consequence of sea level drops. In addition, Brothers
 761 et al. (2012) show varying pockmark depth related to the same hosting layer thickness
 762 (their Fig. 10). A potential explanation is that the field data convolves different stages
 763 of PM development, since the depth (and thus D/h_c) changes with the number of events
 764 N (as we observed experimentally, cf. Fig. 13). We also found a progressive increase in
 765 Type 1 PM width, L , by wall collapse (Fig. 7b), in qualitative agreement with field ob-
 766 servations of PM slopes steeper than the angle of repose, which suggest that these are
 767 active PMs, with temporarily non-stable slopes (Webb et al., 2009). The PM walls ob-
 768 served in our experiments are steeper than in the field (angle of $\sim 10^\circ$ (e.g. Rogers et al.,
 769 2006; Andrews et al., 2010; Schattner et al., 2016)). The steeper PMs in our experiments,
 770 in comparison to field observed PMs, could be due to friction reduction in the field, fol-
 771 lowing multiple seepage events and material degradation at long times in nature (vs. the
 772 short time of our experiments), as well as the artifact of additional frictional resistance
 773 (between the clay and the plexiglass walls) in our quasi-2D setup.

774 5.4 Temporal evolution of gas escape

775 We observe episodic gas escape, with long quiescent periods interspersed by gas bub-
 776 ble ascent (either by deforming plastically the seal, or through fractures). Each seepage
 777 event is accompanied by an abrupt change in PM geometry, and weakening of the flow

778 path (into a pipe). Similar episodic venting was seen in a north sea PM, from which gas
 779 flaring was observed in one expedition but not a few years later (Hustoft et al., 2009).
 780 Long quiescent period of over a decade with no PM geometry change was observed by
 781 (Brothers et al., 2011), implying that it would be extremely hard to observe the short
 782 episodic venting during such periods. However, since previous work suggests that stress
 783 perturbations accelerate bubble escape from sediments (Katsman, 2019), it is not sur-
 784 prising that most observations of episodic gas emission from PMs, follow a stress per-
 785 turbations, e.g. by earthquakes and storms (Hasiotis et al., 1996; Soter, 1999; Field &
 786 Jennings, 1987; Gontz et al., 2001; Christodoulou et al., 2023). Based on our experimen-
 787 tal observations, we hypothesize that episodicity often characterizes gas seepage from
 788 PMs: each seepage event, which also deforms the PM, reflects something akin to a mag-
 789 matic eruption in a volcano: enough gas overpressure must be accumulated to overcome
 790 the overlying layer resistance to deformation and open a fracture, akin to dike opening
 791 by magma. Opening allows gas escape, which then drops the pressure until it again ac-
 792 cumulates to cause another eruption. Finally, we note that magmatic eruptions and mud
 793 volcanoes can also occur in a continuous manner (Kelemen & Aharonov, 1998; Hidalgo
 794 et al., 2015; Fallahi et al., 2017), which, according to the above analogy, suggests a pos-
 795 sibility of continuous gas seepage, which we did not observe in our experiments.

796 6 Conclusions

797 To understand submarine gas seeps and the associated surface deformation creat-
 798 ing pockmarks, we developed an experimental model system composed of a reservoir (glass
 799 beads representing a sandy sediment) overlaid by a deformable seal (clay layer). We find
 800 that gas rises continuously through the reservoir and accumulates in a spatially-limited
 801 zone at the base of the seal, due to the high capillary threshold of the fine-grained clay
 802 limiting gas invasion into it. Over time, sufficient gas overpressure accumulates to de-
 803 form the clay and seep through it. Gas seepage was found to occur by either (i) dom-
 804 ing of the seal and breaching of the dome by fracturing, resulting in disordered, Type-
 805 2, pockmarks; (ii) brittle deformation that creates faults, through which the gas seeps;
 806 or (iii) plastic deformation by gas bubbles ascending through the seal; both (ii) and (iii)
 807 form Type-1 (cone shaped) pockmarks, in thicker, more compliant layers. We also ob-
 808 serve cases where gas seeps as elongated bubbles in faults, representing mixed deforma-
 809 tion mode. The conditions where these deformation modes govern, especially in terms
 810 of layer thickness and consolidation of the layer (determining its stiffness), were computed
 811 theoretically. We find that seepage is often assisted by a positive feedback mechanism:
 812 pipe-like preferential conduits are created by the rise of trains of bubbles, that liquefy
 813 and weaken these conduits. Faults can serve as the starting point for such pathways.

814 We use our table-top experiments to predict natural seepage and deformation by
 815 theoretically extrapolating our finding to field conditions. This analysis suggest that the
 816 initial stage of seal deformation by gas overpressure will create a dome (Fig. 14a, b). Seep-
 817 age is expected to happen by breaching of the dome by mode I fractures leading to Type-
 818 2 pockmark in thin clay layers, and by creation of hydrofractures or by flow through ex-
 819 isting faults that eventually form Type-1 pockmark in thicker clay layers (Fig. 14c). We
 820 hypothesize that as seen experimentally, episodic release of gas bubbles will form pref-
 821 erential conduits (“pipes”) by locally weakening the clay in their passage, as well as pro-
 822 gressively enlarging (in depth and width) a pockmark at the surface (Fig. 14d). Our ex-
 823 perimental observations and theoretical analysis, which are in good agreement with field
 824 data, improves our understanding of natural pockmark formation.

825 *Data Availability Statement*

826 All data used to generate the figures and conclusions in the paper can be down-
 827 loaded from: <https://dx.doi.org/10.6084/m9.figshare.24586926>.

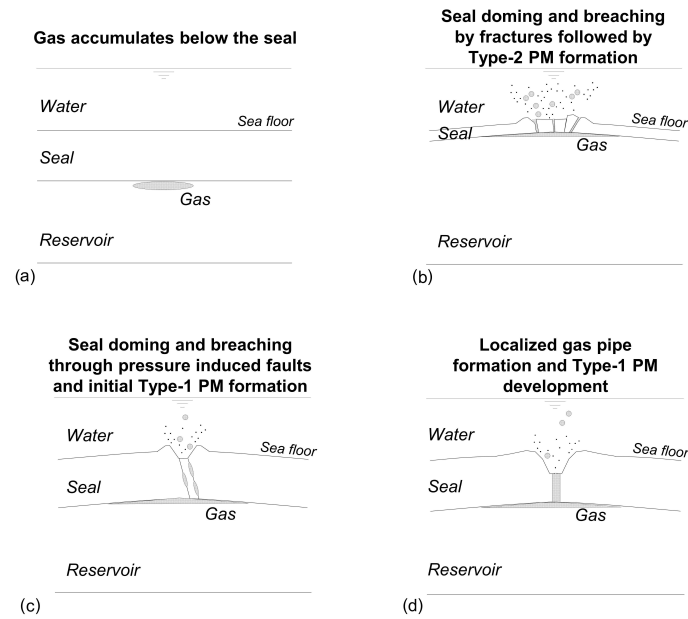


Figure 14: Schematic illustration summarizing the stages of pockmark formation expected in the field, based on theoretical insights from our experiments. (a) Gas accumulates at the top of the reservoir below the seal. Due to overpressure development the seal is deformed by doming, then gas seeps to the sea-floor through the seal in one of the following seal breaching mechanisms: (b) Breaching of the seal by tensional fracturing. Then development of Type 2 pockmark; (c) pressure induced faults (as a consequence of brittle deformation of the seal). In this mechanism, sediment is eroded from the sea-floor and is suspended into the water by the seeping gas (sediment particles are presented as dots), progressively creating a morphological depression (Type 1 pockmark); (d) Eventually, after repeated material degradation (through the pressure induced faults presented in c), localized gas pipe through the seal is created.

828 Acknowledgments

829 RH and EH acknowledge partial support from the Ring Family Foundation for Research
 830 in Atmospheric & Global Changes Studies; RH also acknowledges partial support from
 831 the Israeli Science Foundation (#ISF-867/13), the Israel Ministry of Agriculture and Ru-
 832 rural Development (#821-0137-13), and from the Engineering and Physical Sciences Re-
 833 search Council (EP/V050613/1). OK acknowledges support from the Israeli Science Foun-
 834 dation (#ISF-954/15).

835 References

- 836 Abrams, M. A. (2005). Significance of hydrocarbon seepage relative to petroleum
 837 generation and entrapment. *Marine and Petroleum Geology*, *22*(4), 457–477.
 838 Andresen, K., Dahlin, A., Kjeldsen, K., Røy, H., Bennike, O., Nørgaard-Pedersen,
 839 N., & Seidenkrantz, M.-S. (2021). The longevity of pockmarks—a case study
 840 from a shallow water body in northern Denmark. *Marine Geology*, *434*,
 841 106440.
 842 Andrews, B. D., Brothers, L. L., & Barnhardt, W. A. (2010). Automated feature
 843 extraction and spatial organization of seafloor pockmarks, Belfast Bay, Maine,
 844 USA. *Geomorphology*, *124*(1-2), 55–64.
 845 Archer, D., Buffett, B., & Brovkin, V. (2009). Ocean methane hydrates as a slow

- 846 tipping point in the global carbon cycle. *Proceedings of the National Academy*
 847 *of Sciences*, 106(49), 20596–20601.
- 848 Atkinson, J., Charles, J., & Mhach, H. (1994). Undrained hydraulic fracture in cav-
 849 ity expansion tests. In *International conference on soil mechanics and founda-*
 850 *tion engineering* (pp. 1009–1012).
- 851 Barry, M. A., Boudreau, B. P., & Johnson, B. D. (2012). Gas domes in soft cohesive
 852 sediments. *Geology*, 40(4), 379–382. doi: 10.1130/G32686.1
- 853 Bayon, G., Loncke, L., Dupré, S., Caprais, J.-C., Ducassou, E., Duperron, S., ...
 854 others (2009). Multi-disciplinary investigation of fluid seepage on an unstable
 855 margin: the case of the central Nile deep sea fan. *Marine Geology*, 261(1–4),
 856 92–104.
- 857 Berndt, C. (2005). Focused fluid flow in passive continental margins. *Philosophical*
 858 *Transactions of the Royal Society A: Mathematical, Physical and Engineering*
 859 *Sciences*, 363(1837), 2855–2871. doi: 10.1098/rsta.2005.1666
- 860 Berndt, C., Bünz, S., & Mienert, J. (2003). Polygonal fault systems on the mid-
 861 norwegian margin: a long-term source for fluid flow. *Geological Society, Lon-*
 862 *don, Special Publications*, 216(1), 283–290.
- 863 Bøe, R., Rise, L., & Ottesen, D. (1998). Elongate depressions on the southern slope
 864 of the Norwegian trench (Skagerrak): morphology and evolution. *Marine Geol-*
 865 *ogy*, 146(1–4), 191–203.
- 866 Böttner, C., Berndt, C., Reinardy, B. T., Geersen, J., Karstens, J., Bull, J. M.,
 867 ... Haeckel, M. (2019). Pockmarks in the witch ground basin, central
 868 north sea. *Geochemistry, Geophysics, Geosystems*, 20(4), 1698–1719. doi:
 869 <https://doi.org/10.1029/2018GC008068>
- 870 Boudreau, B. P. (2012). The physics of bubbles in surficial, soft, cohesive sediments.
 871 *Marine and Petroleum Geology*, 38(1), 1–18.
- 872 Boudreau, B. P., Algar, C., Johnson, B. D., Croudace, I., Reed, A., Furukawa, Y.,
 873 ... Gardiner, B. (2005). Bubble growth and rise in soft sediments. *Geology*,
 874 33(6), 517–520.
- 875 Bower, A. F. (2009). *Applied mechanics of solids*. CRC press.
- 876 Brothers, L. L., Kelley, J. T., Belknap, D. F., Barnhardt, W. A., Andrews, B. D.,
 877 Legere, C., & Clarke, J. E. H. (2012). Shallow stratigraphic control on pock-
 878 mark distribution in north temperate estuaries. *Marine Geology*, 329, 34–45.
- 879 Brothers, L. L., Kelley, J. T., Belknap, D. F., Barnhardt, W. A., Andrews, B. D.,
 880 & Maynard, M. L. (2011). More than a century of bathymetric observations
 881 and present-day shallow sediment characterization in Belfast Bay, Maine, USA:
 882 Implication for pockmark field longevity. *Geo-Marine Letters*, 31, 237–248.
- 883 Brown, K. M. (1990). The nature and hydrogeologic significance of mud diapirs
 884 and diatremes for accretionary systems. *Journal of Geophysical Research: Solid*
 885 *Earth*, 95(B6), 8969–8982.
- 886 Camerlenghi, A., Cita, M., Vedova, B. D., Fusi, N., Mirabile, L., & Pellis, G. (1995).
 887 Geophysical evidence of mud diapirism on the Mediterranean ridge accre-
 888 tionary complex. *Marine Geophysical Researches*, 17(2), 115–141.
- 889 Cartwright, J., Huuse, M., & Aplin, A. (2007). Seal bypass systems. *AAPG bulletin*,
 890 91(8), 1141–1166.
- 891 Cartwright, J., & Santamarina, C. (2015). Seismic characteristics of fluid es-
 892 cape pipes in sedimentary basins: implications for pipe genesis. *Marine and*
 893 *Petroleum Geology*, 65, 126–140.
- 894 Cathles, L. M., Su, Z., & Chen, D. (2010). The physics of gas chimney and pock-
 895 mark formation, with implications for assessment of seafloor hazards and gas
 896 sequestration. *Marine and Petroleum Geology*, 27, 82–91.
- 897 Chapuis, R. P., & Aubertin, M. (2003). On the use of the Kozeny-Carman equation
 898 to predict the hydraulic conductivity of soils. *Canadian Geotechnical Journal*,
 899 40(3), 616–628.
- 900 Christodoulou, D., Papatheodorou, G., Geraga, M., Etiope, G., Giannopoulos, N.,

- 901 Kokkalas, S., ... others (2023). Geophysical and geochemical exploration of
 902 the pockmark field in the gulf of patras: New insights on formation, growth
 903 and activity. *Applied Sciences*, 13(18), 10449.
- 904 Crutchley, G. J., Mountjoy, J. J., Hillman, J. I. T., Turco, F., Watson, S., Flem-
 905 ings, P. B., ... Bialas, J. (2021). Upward-doming zones of gas hydrate
 906 and free gas at the bases of gas chimneys, new zealand's hikurangi margin.
 907 *Journal of Geophysical Research: Solid Earth*, 126(9), e2020JB021489. doi:
 908 <https://doi.org/10.1029/2020JB021489>
- 909 Davies, R. J., Mathias, S. A., Moss, J., Hustoft, S., & Newport, L. (2012). Hydraulic
 910 fractures: How far can they go? *Marine and petroleum geology*, 37(1), 1–6.
- 911 de Mahiques, M. M., Schattner, U., Lazar, M., Sumida, P. Y. G., & de Souza,
 912 L. A. P. (2017). An extensive pockmark field on the upper atlantic margin
 913 of southeast brazil: spatial analysis and its relationship with salt diapirism.
 914 *Heliyon*, 3(2), e00257.
- 915 Dickens, G. R. (n.d.). Rethinking the global carbon cycle with a large, dynamic and
 916 microbially mediated gas hydrate capacitor. *Earth and Planetary Science Let-
 917 ters*.
- 918 Dillon, W. P., Danforth, W., Hutchinson, D., Drury, R., Taylor, M., & Booth, J.
 919 (1998). Evidence for faulting related to dissociation of gas hydrate and release
 920 of methane off the southeastern united states. *Geological Society, London,
 921 Special Publications*, 137(1), 293–302.
- 922 Dupré, S., Woodside, J., Klaucke, I., Mascle, J., & Foucher, J.-P. (2010).
 923 Widespread active seepage activity on the nile deep sea fan (offshore egypt)
 924 revealed by high-definition geophysical imagery. *Marine Geology*, 275(1),
 925 1–19.
- 926 Fallahi, M. J., Obermann, A., Lupi, M., Karyono, K., & Mazzini, A. (2017). The
 927 plumbing system feeding the lusi eruption revealed by ambient noise tomogra-
 928 phy. *Journal of Geophysical Research: Solid Earth*, 122(10), 8200–8213. doi:
 929 <https://doi.org/10.1002/2017JB014592>
- 930 Fauria, K. E., & Rempel, A. W. (2011). Gas invasion into water-saturated, uncon-
 931 solidated porous media: Implications for gas hydrate reservoirs. *Earth Planet.
 932 Sci. Lett.*, 312(1–2), 188–193.
- 933 Field, M. E., & Jennings, A. E. (1987). Seafloor gas seeps triggered by a northern
 934 california earthquake. *Marine Geology*, 77(1–2), 39–51.
- 935 Forwick, M., Baeten, N. J., & Vorren, T. O. (2009). Pockmarks in spitsbergen
 936 fjords. *Norwegian Journal of Geology/Norsk Geologisk Forening*, 89.
- 937 Franchi, F., Rovere, M., Gamberi, F., Rashed, H., Vaselli, O., & Tassi, F. (2017).
 938 Authigenic minerals from the Paola Ridge (southern Tyrrhenian Sea): Ev-
 939 idences of episodic methane seepage. *Marine and Petroleum Geology*, 86,
 940 228–247. doi: <https://doi.org/10.1016/j.marpetgeo.2017.05.031>
- 941 García-Gil, S. (2003). A natural laboratory for shallow gas: the rías baixas (nw
 942 spain). *Geo-Marine Letters*, 23(3), 215–229.
- 943 Gay, A., Lopez, M., Cochonat, P., Séranne, M., Levaché, D., & Sermondadaz, G.
 944 (2006). Isolated seafloor pockmarks linked to BSRs, fluid chimneys, polygonal
 945 faults and stacked Oligocene-Miocene turbiditic palaeochannels in the Lower
 946 Congo Basin. *Marine Geology*, 226(1–2), 25–40.
- 947 Goff, J. A. (2019). Modern and fossil pockmarks in the new england mud patch:
 948 Implications for submarine groundwater discharge on the middle shelf. *Geo-
 949 physical Research Letters*, 46(21), 12213–12220. doi: [https://doi.org/10.1029/
 950 2019GL084881](https://doi.org/10.1029/2019GL084881)
- 951 Gontz, A. M., Belknap, D., Daniel, F., & Kelley, J. (2001). Evidence for changes
 952 in the belfast bay pockmark field, maine. In *Geological society of america, ab-
 953 stracts with programs* (Vol. 33).
- 954 Harrington, P. (1985). Formation of pockmarks by pore-water escape. *Geo-Marine
 955 Letters*, 5(3), 193–197.

- 956 Hasiotis, T., Papatheodorou, G., Kastanos, N., & Ferentinos, G. (1996). A pock-
 957 mark field in the patras gulf (greece) and its activation during the 14/7/93
 958 seismic event. *Marine Geology*, *130*(3-4), 333–344.
- 959 Hidalgo, S., Battaglia, J., Arellano, S., Steele, A., Bernard, B., Bourquin, J., ...
 960 Vasconez, F. (2015). SO₂ degassing at Tungurahua volcano (Ecuador)
 961 between 2007 and 2013: Transition from continuous to episodic activity.
 962 *J. Volcanol. Geotherm. Res.*, *298*, 1–14. doi: [https://doi.org/10.1016/
 963 j.jvolgeores.2015.03.022](https://doi.org/10.1016/j.jvolgeores.2015.03.022)
- 964 Holtzman, R., Szulczewski, M. L., & Juanes, R. (2012). Capillary fracturing in gran-
 965 ular media. *Physical Review Letters*, *108*(26), 264504.
- 966 Hornbach, M. J., Saffer, D. M., & Holbrook, W. S. (2004). Critically pressured free-
 967 gas reservoirs below gas-hydrate provinces. *Nature*, *427*(6970), 142–4. doi: 10
 968 .1038/nature02172
- 969 Hovland, M., Gardner, J., & Judd, A. (2002). The significance of pockmarks to un-
 970 derstanding fluid flow processes and geohazards. *Geofluids*, *2*(2), 127–136.
- 971 Hovland, M., Hegglund, R., De Vries, M., & Tjelta, T. (2010). Unit-pockmarks and
 972 their potential significance for predicting fluid flow. *Marine and Petroleum Ge-
 973 ology*, *27*(6), 1190–1199.
- 974 Hovland, M., Judd, A. G., & Burke, R. (1993). The global flux of methane from
 975 shallow submarine sediments. *Chemosphere*, *26*(1), 559–578.
- 976 Hovland, M., & Sommerville, J. H. (1985). Characteristics of two natural gas seep-
 977 ages in the north sea. *Marine and Petroleum Geology*, *2*(4), 319–326.
- 978 Hovland, M., Svensen, H., Forsberg, C. F., Johansen, H., Fichler, C., Fosså, J. H.,
 979 ... Rueslåtten, H. (2005). Complex pockmarks with carbonate-ridges off mid-
 980 norway: products of sediment degassing. *Marine geology*, *218*(1-4), 191–206.
- 981 Hsu, C.-W., Marcon, Y., Römer, M., Pape, T., Klauke, I., Loher, M., ...
 982 Bohrmann, G. (2021). Heterogeneous hydrocarbon seepage at mictlan as-
 983 phalt knoll of the southern gulf of mexico. *Marine and Petroleum Geology*,
 984 105185.
- 985 Hustoft, S., Bünz, S., Mienert, J., & Chand, S. (2009). Gas hydrate reservoir and
 986 active methane-venting province in sediments on 20 Ma young oceanic crust in
 987 the Fram Strait, offshore NW-Svalbard. *Earth and Planetary Science Letters*,
 988 *284*(1-2), 12–24.
- 989 Hustoft, S., Mienert, J., Bünz, S., & Nouzé, H. (2007). High-resolution 3d-seismic
 990 data indicate focussed fluid migration pathways above polygonal fault systems
 991 of the mid-norwegian margin. *Marine Geology*, *245*(1-4), 89–106.
- 992 Jain, A. K., & Juanes, R. (2009). Preferential mode of gas invasion in sediments:
 993 grain-scale mechanistic model of coupled multiphase fluid flow and sediment
 994 mechanics. *Journal of Geophysical Research: Solid Earth*, *114*, B08101.
- 995 Jedari-Eyvazi, F., Bayrakci, G., Minshull, T. A., Bull, J. M., Henstock, T. J., Mac-
 996 donald, C., & Robinson, A. H. (2023). Seismic characterization of a fluid
 997 escape structure in the North Sea: the Scanner Pockmark complex area. *Geo-
 998 physical Journal International*, *234*(1), 597–619. doi: 10.1093/gji/ggad078
- 999 Judd, A., & Hovland, M. (2009). *Seabed fluid flow: the impact on geology, biology
 1000 and the marine environment*. Cambridge University Press.
- 1001 Judd, A. G. (2003). The global importance and context of methane escape from the
 1002 seabed. *Geo-Marine Letters*, *23*(3), 147–154.
- 1003 Katsman, R. (2019). Methane bubble escape from gas horizon in muddy aquatic
 1004 sediment under periodic wave loading. *Geophysical Research Letters*, *46*(12),
 1005 6507–6515. doi: 10.1029/2019GL083100
- 1006 Kelemen, P. B., & Aharonov, E. (1998). Periodic formation of magma fractures
 1007 and generation of layered gabbros in the lower crust beneath oceanic spreading
 1008 ridges. *Geophysical monograph*, *106*, 267–289.
- 1009 King, L. H., & MacLean, B. (1970). Pockmarks on the scotian shelf. *Geological Soci-
 1010 ety of America Bulletin*, *81*(10), 3141–3148.

- 1011 Koch, S., Berndt, C., Bialas, J., Haeckel, M., Crutchley, G., Papenberg, C., ...
 1012 Greinert, J. (2015). Gas-controlled seafloor doming. *Geology*, *43*(7), 571–574.
- 1013 Krämer, K., Holler, P., Herbst, G., Bratek, A., Ahmerkamp, S., Neumann, A., ...
 1014 Winter, C. (2017). Abrupt emergence of a large pockmark field in the german
 1015 bight, southeastern north sea. *Scientific Reports*, *7*(1), 1–8.
- 1016 Lawal, M. A., Bialik, O. M., Lazar, M., Waldmann, N. D., Foubert, A., & Makovsky,
 1017 Y. (2023). Modes of gas migration and seepage on the salt-rooted palmahim
 1018 disturbance, southeastern mediterranean. *Marine and Petroleum Geology*, *153*,
 1019 106256. doi: <https://doi.org/10.1016/j.marpetgeo.2023.106256>
- 1020 Linke, P., Pfannkuche, O., Torres, M., Collier, R., Witte, U., McManus, J., ...
 1021 Nakamura, K.-i. (1999). Variability of benthic flux and discharge rates at vent
 1022 sites determined by in situ instruments. *EOS transactions*, *80*(46 Fall Meet.
 1023 Suppl), F509.
- 1024 Loncke, L., & Mascle, J. F. S. P. (2004). Mud volcanoes, gas chimneys, pockmarks
 1025 and mounds in the Nile deep-sea fan (eastern mediterranean): geophysical
 1026 evidences,. *Marine and Petroleum Geology*, *21*(6), 669–689.
- 1027 Løseth, H., Wensaas, L., Arntsen, B., Hanken, N.-M., Basire, C., & Graue, K.
 1028 (2011). 1000 m long gas blow-out pipes. *Marine and Petroleum Geology*,
 1029 *28*(5), 1047–1060.
- 1030 Macelloni, L., Simonetti, A., Knapp, J. H., Knapp, C. C., Lutken, C. B., & Lapham,
 1031 L. L. (2012). Multiple resolution seismic imaging of a shallow hydrocar-
 1032 bon plumbing system, woolsey mound, northern gulf of Mexico. *Marine and*
 1033 *Petroleum Geology*, *38*(1), 128–142.
- 1034 Makhnenko, R., Vilarrasa, V., Mylnikov, D., & Laloui, L. (2017). Hydromechan-
 1035 ical aspects of CO₂ breakthrough into clay-rich caprock. *Energy Procedia*,
 1036 *114*, 3219–3228. (13th International Conference on Greenhouse Gas Control
 1037 Technologies, GHGT-13, 14–18 November 2016, Lausanne, Switzerland) doi:
 1038 <https://doi.org/10.1016/j.egypro.2017.03.1453>
- 1039 Marchi, M., Gottardi, G., & Soga, K. (2014). Fracturing pressure in clay. *Journal*
 1040 *of Geotechnical and Geoenvironmental Engineering*, *140*(2), 04013008. doi: 10
 1041 .1061/(ASCE)GT.1943-5606.0001019
- 1042 Marcon, Y., Kelley, D., Thornton, B., Manalang, D., & Bohrmann, G. (2021). Vari-
 1043 ability of natural methane bubble release at southern hydrate ridge. *Geochem-*
 1044 *istry, Geophysics, Geosystems*, *22*(10), e2021GC009894. doi: [https://doi.org/](https://doi.org/10.1029/2021GC009894)
 1045 [10.1029/2021GC009894](https://doi.org/10.1029/2021GC009894)
- 1046 Mayne, P. W. (2001). Stress-strain-strength-flow parameters from enhanced in-situ
 1047 tests. In *Proc. Int. Conf. on In situ measurement of soil properties and case*
 1048 *histories, Bali* (pp. 27–47).
- 1049 Mazzini, A., Ivanov, M. K., Nermoen, A., Bahr, A., Bohrmann, G., Svensen, H., &
 1050 Planke, S. (2008). Complex plumbing systems in the near subsurface: Geome-
 1051 tries of authigenic carbonates from Dolgovskoy mound (Black Sea) constrained
 1052 by analogue experiments. *Marine and Petroleum Geology*, *25*(6), 457–472. doi:
 1053 <https://doi.org/10.1016/j.marpetgeo.2007.10.002>
- 1054 McGinnis, D. F., Greinert, J., Artemov, Y., Beaubien, S. E., & Wüest, a. (2006).
 1055 Fate of rising methane bubbles in stratified waters: How much methane
 1056 reaches the atmosphere? *Journal of Geophysical Research: Solid Earth*,
 1057 *111*(C9), 1–15. doi: [10.1029/2005JC003183](https://doi.org/10.1029/2005JC003183)
- 1058 Morel-Seytoux, H. J. (1993). Capillary barrier at the interface of two layers. In
 1059 D. Russo & G. Dagan (Eds.), *Water flow and solute transport in soils: De-*
 1060 *velopments and applications* (pp. 136–151). Springer Berlin Heidelberg. doi:
 1061 [10.1007/978-3-642-77947-3_10](https://doi.org/10.1007/978-3-642-77947-3_10)
- 1062 Moss, J., & Cartwright, J. (2010). The spatial and temporal distribution of pipe for-
 1063 mation, offshore Namibia. *Marine and Petroleum Geology*, *27*(6), 1216–1234.
- 1064 Nermoen, A., Galland, O., Jettestuen, E., Fristad, K., Podladchikov, Y., Svensen,
 1065 H., & Malthes-Sørensen, A. (2010). Experimental and analytic model-

- ing of piercement structures. *Journal of Geophysical Research: Solid Earth*, 115(B10). doi: <https://doi.org/10.1029/2010JB007583>
- Neuzil, C. E. (1994). How permeable are clays and shales? *Water Resources Research*, 30(2), 145-150. doi: <https://doi.org/10.1029/93WR02930>
- Osborne, M. J., & Swarbrick, R. E. (1997). Mechanisms for Generating Overpressure in Sedimentary Basins: A Reevaluation1. *AAPG Bulletin*, 81(6), 1023-1041. doi: 10.1306/522B49C9-1727-11D7-8645000102C1865D
- Perrin, H., Clavaud, C., Wyart, M., Metzger, B., & Forterre, Y. (2019, Aug). Interparticle friction leads to nonmonotonic flow curves and hysteresis in viscous suspensions. *Physical Review X*, 9, 031027. doi: 10.1103/PhysRevX.9.031027
- Pilcher, R., & Argent, J. (2007). Mega-pockmarks and linear pockmark trains on the west african continental margin. *Marine Geology*, 244(1), 15-32.
- Plaza-Faverola, A., Bünz, S., & Mienert, J. (2011). Repeated fluid expulsion through sub-seabed chimneys offshore norway in response to glacial cycles. *Earth and Planetary Science Letters*, 305(3-4), 297-308.
- Plaza-Faverola, A., Westbrook, G. K., Ker, S., Exley, R. J., Gailler, A., Minshull, T. A., & Broto, K. (2010). Evidence from three-dimensional seismic tomography for a substantial accumulation of gas hydrate in a fluid-escape chimney in the nyegga pockmark field, offshore norway. *Journal of Geophysical Research: Solid Earth*, 115(B8).
- Poryles, R., Vidal, V., & Varas, G. (2016). Bubbles trapped in a fluidized bed: Trajectories and contact area. *Physical Review E*, 93, 032904. doi: 10.1103/PhysRevE.93.032904
- Ramos, G., Varas, G., Géminard, J.-C., & Vidal, V. (2015). Gas-induced fluidization of mobile liquid-saturated grains. *Physical Review E*, 92, 062210. doi: 10.1103/PhysRevE.92.062210
- Räss, L., Simon, N. S., & Podladchikov, Y. Y. (2018). Spontaneous formation of fluid escape pipes from subsurface reservoirs. *Scientific Reports*, 8(1), 11116.
- Riboulot, V., Sultan, N., Imbert, P., & Ker, S. (2016). Initiation of gas-hydrate pockmark in deep-water nigeria: Geo-mechanical analysis and modelling. *Earth and Planetary Science Letters*, 434, 252-263.
- Riedel, M., Villinger, H., Freudenthal, T., Pape, T., Bünz, S., & Bohrmann, G. (2020). Thermal characterization of pockmarks across vestnesa and svyatogor ridges, offshore svalbard. *Journal of Geophysical Research: Solid Earth*, 125(12), e2020JB019468. doi: 10.1029/2020JB019468
- Rogers, J. N., Kelley, J. T., Belknap, D. F., Gontz, A., & Barnhardt, W. A. (2006). Shallow-water pockmark formation in temperate estuaries: a consideration of origins in the western gulf of maine with special focus on belfast bay. *Marine Geology*, 225(1-4), 45-62.
- Schattner, U., Lazar, M., Harari, D., & Waldmann, N. (2012). Active gas migration systems offshore northern Israel, first evidence from seafloor and subsurface data. *Continental Shelf Research*, 48, 167-172. doi: 10.1016/j.csr.2012.08.003
- Schattner, U., Lazar, M., Souza, L., Ten Brink, U., & Mahiques, M. (2016). Pockmark asymmetry and seafloor currents in the santos basin offshore brazil. *Geo-Marine Letters*, 36(6), 457-464.
- Simonetti, A., Knapp, J. H., Sleeper, K., Lutken, C. B., Macelloni, L., & Knapp, C. C. (2013). Spatial distribution of gas hydrates from high-resolution seismic and core data, woolsey mound, northern gulf of mexico. *Marine and Petroleum Geology*, 44, 21-33.
- Skarke, A., Ruppel, C., Kodis, M., Brothers, D., & Lobecker, E. (2014). Widespread methane leakage from the sea floor on the northern us atlantic margin. *Nature Geoscience*, 7(9), 657-661.
- Soter, S. (1999). Macroscopic seismic anomalies and submarine pockmarks in the corinth-patras rift, greece. *Tectonophysics*, 308(1-2), 275-290.
- Sultan, N., Marsset, B., Ker, S., Marsset, T., Voisset, M., Vernant, a. M., ... Dra-

- 1121 peau, D. (2010). Hydrate dissolution as a potential mechanism for pockmark
1122 formation in the Niger delta. *Journal of Geophysical Research: Solid Earth*,
1123 115(B8), 1–33. doi: 10.1029/2010JB007453
- 1124 Sun, Q., Wu, S., Cartwright, J., & Dong, D. (2012). Shallow gas and focused fluid
1125 flow systems in the pearl river mouth basin, northern south china sea. *Marine*
1126 *Geology*, 315, 1–14.
- 1127 Sun, Z., & Santamarina, J. C. (2019). Grain-displacive gas migration in fine-grained
1128 sediments. *Journal of Geophysical Research: Solid Earth*, 124(3), 2274–2285.
1129 doi: 10.1029/2018JB016394
- 1130 Svensen, H., Planke, S., Malthes-Sørensen, A., Jamtveit, B., Myklebust, R., Eidem,
1131 T. R., & Rey, S. S. (2004). Release of methane from a volcanic basin as a
1132 mechanism for initial eocene global warming. *Nature*, 429(6991), 542–545.
- 1133 Tary, J.-B., Geli, L., Guennou, C., Henry, P., Sultan, N., Çağatay, N., & Vi-
1134 dal, V. (2012). Microevents produced by gas migration and expulsion
1135 at the seabed: a study based on sea bottom recordings from the sea of
1136 marmara. *Geophysical Journal International*, 190(2), 993–1007. doi:
1137 10.1111/j.1365-246X.2012.05533.x
- 1138 Turcotte, D., & Schubert, G. (2014). *Geodynamics* (3rd ed.). Cambridge University
1139 Press. doi: 10.1017/CBO9780511843877
- 1140 Ugural, A. (1999). *Stresses in plates and shells*. WCB/McGraw Hill.
- 1141 Varas, G., Vidal, V., & Géminard, J.-C. (2009). Dynamics of crater formations in
1142 immersed granular materials. *Physical Review E*, 79(2), 1–7.
- 1143 Varas, G., Vidal, V., & Géminard, J.-C. (2011). Venting dynamics of an immersed
1144 granular layer. *Physical Review E*, 83(1), 1–6.
- 1145 Volfson, D., Tsimring, L. S., & Aranson, I. S. (2003, Aug). Partially fluidized shear
1146 granular flows: Continuum theory and molecular dynamics simulations. *Physi-
1147 cal Review E*, 68, 021301. doi: 10.1103/PhysRevE.68.021301
- 1148 Webb, K. E., Hemmer, O., Lepland, A., & Gray, J. S. (2009). Pockmarks in the in-
1149 ner oslofjord, norway. *Geo-Marine Letters*, 29, 111–124.
- 1150 Westbrook, G. K., Thatcher, K. E., Rohling, E. J., Piotrowski, A. M., Pälike, H.,
1151 Osborne, A. H., ... Aquilina, A. (2009). Escape of methane gas from the
1152 seabed along the West Spitsbergen continental margin. *Geophysical Research*
1153 *Letters*, 36(15), L15608.
- 1154 Wood, D. M. (1991). *Soil behaviour and critical state soil mechanics*. Cambridge
1155 University Press. doi: 10.1017/CBO9781139878272
- 1156 Wu, H., & Pollard, D. D. (1995). An experimental study of the relationship be-
1157 tween joint spacing and layer thickness. *Journal of Structural Geology*, 17(6),
1158 887–905.